Marion Ranaivombola, Nelson Bègue, Hassan Bencherif, Tristan Millet, Venkataraman Sivakumar, Valentin Duflot, Alexandre Baron, Nkanyiso Mbatha, Stuart Piketh, Paola Formenti, et al.

Article

Aerosol Optical Properties and Types over Southern Africa and Reunion Island Determined from Ground-Based and Satellite Observations over a 13-Year Period (2008–2021)

Marion Ranaivombola [1,*], **Nelson Bègue** [1], **Hassan Bencherif** [1,2], **Tristan Millet** [1], **Venkataraman Sivakumar** [2,3], **Valentin Duflot** [1], **Alexandre Baron** [1,4,5], **Nkanyiso Mbatha** [6], **Stuart Piketh** [7], **Paola Formenti** [8] and **Philippe Goloub** [9]

[1] Laboratoire de l'Atmosphère et des Cyclones (LACy), UMR 8105 CNRS, Université de La Réunion, Météo-France, F-97400 Saint-Denis de La Réunion, France
[2] The Discipline of Physics, School of Chemistry and Physics, College of Agriculture, Engineering and Science, Westville Campus, University of KwaZulu Natal, Durban 4000, South Africa
[3] National Institute for Theoretical and Computational Sciences, University of KwaZulu Natal, Durban 4000, South Africa
[4] Cooperative Institute for Research in Environmental Sciences, CU Boulder, Boulder, CO 80309, USA
[5] NOAA Chemical Sciences Laboratory, Boulder, CO 80305, USA
[6] Department of Geography, University of Zululand, KwaDlangezwa 3886, South Africa
[7] Unit for Environmental Science and Management, North-West University, Potchefstroom 2520, South Africa
[8] Université Paris Cité and Univ Paris Est Creteil, CNRS, LISA, F-75013 Paris, France
[9] UMR 8518—LOA—Laboratoire d'Optique Atmosphérique, University of Lille, F-59000 Lille, France
* Correspondence: marion.ranaivombola@univ-reunion.fr

Abstract: Fires occur seasonally in Southern Africa, from June to November, increasing tropospheric aerosol loading and triggering harmful consequences for the environment and human health. This study aims to examine 13 years of aerosol optical characteristics and types over Southern Africa and Reunion Island. Using AERONET sun photometers and MODIS observations, we found that a high aerosol optical depth and Angström exponent are associated with two predominant types of aerosols (biomass burning/urban industrial and mixed type) throughout the spring season. According to CALIOP observations, the major aerosol types with occurrence frequencies above 10% are polluted continental/smoke, polluted dust, and elevated smoke, whereas dust, clean continental, and dusty marine have occurrence frequencies below 1%. In comparison to other seasons, the vertical profiles of elevated smoke have different shapes in spring, with a seasonal shift in the peak altitude (from 3–4 km), when fire activity is at its maximum. At these altitudes, the northern regions presented occurrence frequencies of 32% on average, while lower values were found for the southern or farthest regions (<10–20% on average). The Lagrangian HYSPLIT model back-trajectories demonstrated eastward transport, with air masses from South America and the Atlantic Ocean that recirculate around the study sites. The aerosols are mainly derived from active biomass burning areas near the study sites and, to a lesser extent, from remote sources such as South America.

Keywords: AOD; aerosol type; AERONET; MODIS; CALIOP; biomass burning season

1. Introduction

Fires occur in many parts of the world and are associated with atmospheric emissions from the boundary layer to the lower stratosphere. Such aerosol and gas emissions trigger impacts on both climate and air quality, and are therefore harmful to human health [1]. Southern Africa is one of the regions in the southern hemisphere where there is prevalent biomass burning activity. Most of the fire activity in this region is not due to natural causes but the result of agricultural burning associated with subsistence agriculture and livestock grazing [2]. The analysis of thermal anomalies and burned areas reveals that

fires occur seasonally in Southern Africa between June and November [3,4]. Savanna fires are dominant in terms of soil type and represent 90% of the total burned area [5]. Using multisource remotely sensed data, Kganyago et al. [6] emphasized that grassland is largely burned during the austral winter (from June to August) and spring (from September to November) seasons, with a total burned area of around 306 thousand and 208 thousand km^2, respectively. Southern African air flows are governed by five common trajectories: direct easterly or westerly transport; easterly or westerly advection out of an initially anticyclonic circulation; and anticyclonic recirculation [7]. Anticyclonic circulation creates stable inversion layers over biomass burning regions. These stable layers can trap aerosols and trace gases, leading to recirculation of emissions in the anticyclonic gyre, resulting in increased pollution.

Several measurement campaigns have been undertaken in order to analyze and characterize the transport of biomass burning aerosols in Africa (Southern Africa Fire-Atmosphere Research Initiative (SAFARI-1992 and SAFARI-2000) [8–10], AErosol, RadiatiOn and CLOuds in Southern Africa (AEROCLO-sA) [11], Namib Fog Life Cycle Analysis (NaFoLiCA) [12], and Observations of Aerosols above Clouds and Their Interactions (ORACLES) [13–15]. These previous campaigns are scientifically complementary in providing a large-scale picture of aerosols and their interactions with clouds and fog, and specifically of biomass burning plumes at or near emissions (AEROCLO-sA and NaFoLiCa) and short-to-mid-range transport (AEROCLO-sA and ORACLES). The ground-based and airborne measurements carried out in the SAFARI field campaign are aimed at obtaining new insights into the transport of biomass burning plumes at a regional scale [9]. In the framework of SAFARI-2000, Schmid et al. [16] reported the presence of "massive, thick aerosol layers" covering Southern Africa during the biomass burning season. These thick aerosol layers containing smoke and haze formed a river of smoke that crossed the subcontinent and exited from southeastern Southern Africa. Based on data collected during the AEROCLO-sA field campaign in Southern Africa and a meso-scale model, [17] investigated the formation and transport of this river of smoke over Southern Africa. Their results suggest that the interaction between the tropical temperate troughs and the cut-off lows, which form during winter on the west coast of Africa, may have a role in promoting the transport of biomass burning aerosols from fire-prone regions in the tropical band to the temperate mid-latitudes. The ORACLES field campaign was conducted with the aim of providing the most extensive efforts in measurement for the broader southern Atlantic region since SAFARI-2000. In particular, the ORACLES campaign was designed to investigate how biomass burning aerosols interact with oceanic stratocumulus clouds and how such an interaction affects the radiation budget [13–15].

In these previous studies, it was pointed out that the biomass burning plume crosses Southern Africa during the dry season (from July to November). Therefore, the transport of biomass burning plume induces significant variability of aerosol and chemical species over Southern Africa. Analysis of sun photometer measurements over Southern Africa revealed a significant increase in aerosol optical depth (AOD) during the biomass burning season (which extends from August to November, with the most intense fire activity occurring in the spring season) [18–27]. The few studies that the vertical distribution of aerosol from ground-based and spaceborne lidar revealed that the top aerosol layer ranges from 3.5 to 5.7 km during the biomass burning season [7,28,29]. Most recently, the evolution of the vertical distribution and optical properties of aerosols in the free troposphere was characterized for the first time over the Namibian coast during the AEROCLO-sA field campaign by Chazette et al. [30]; based on ground-based, airborne, and spaceborne lidar measurements around the Henties Bay supersite, they showed that aerosols were transported up to 6 km above mean sea level and associated with an increase in AOD (from 0.2 to 0.7).

The common point among the aforementioned studies is their interest in the western coast of Southern Africa and the transport of biomass burning plumes into the southeast Atlantic Ocean. A few studies have been carried out on the transport of the African biomass

burning plume in terms of the vertical distribution of aerosols and trace gases over the South-West Indian Ocean (SWIO) basin [2,31–34]. Based on ozone observations from radiosondes and lidar observations, Clain et al. [31] found an increase in the tropospheric ozone over Reunion Island during the dry season, in phase with biomass burning activity in Southern Africa. Most recently, Duflot et al. [35] conducted an evaluation that revealed the main contributor to AOD variability over Reunion Island to be biomass burning activity in Southern Africa. Most previous works on the variability of aerosols during the biomass burning season undertaken in Southern Africa were conducted on a local scale (such as Durban, Skukuza, Cape Town, and Henties Bay). The work of Horowitz et al. [36] is the most recent of those dedicated to the entire African continent in which sun photometer observations from the AErosol RObotic NETwork (AERONET) network were combined with a numerical model. Nonetheless, this work only included three sites in southern Africa. The usefulness of sun photometry measurements from the AERONET network for a preliminary estimation of the main type of aerosol has been reported in numerous works [19,22,23,37,38].

Southern Africa has a complex aerosol composition due to the variety of possible sources [39,40]. Natural aerosols are mainly composed of marine spray, due to the strong productivity in coastal areas, and mineral dust aerosols. The latter are formed throughout the western desert and semi desert areas as well as in wetter e astern parts of South Africa wherever bare or sparsely covered dry ground is found [39,41]. Regional anthropogenic pollution is related to large urban areas elsewhere in South Africa as well as over the central plateau of Highveld [39,42]. Previous works have shown that aerosols from burning areas in Central Africa (biomass burning occurring to the north of 20°S) contribute significantly to the African haze layer [39,40,43]. Southern Africa is the region hosting major transport of biomass burning sources in Central Africa [44]. The analysis of this very complex mixture of aerosols is crucial for the investigation of their radiative effect over Southern Africa.

The aforementioned reasons serve as inspiration for our work, which aims to investigate the variability of the aerosol optical properties and types across several selected sites in Southern Africa and Reunion during the biomass burning season.

In summary, the objectives of this work are as follows:

1. Provide an overview and update on the spatiotemporal variability of aerosol optical properties and types across several selected sites in Southern Africa and Reunion.
2. Discuss the vertical distribution of aerosol.
3. Investigate the origin of air masses over the selected sites.

The paper is organized as follows: The datasets used in this study are presented in Section 2 along with a description of the selected sites and the methodology. The spatiotemporal optical properties and types of aerosols in Southern Africa and Reunion are presented in Section 3.1, wherein we use the 3D distribution of aerosol type based on CALIOP to obtain the vertical distribution of each type as a function of altitude. The findings are provided in Section 3.2 and used to initiate HYSPLIT (Hybrid Single-Particle Lagrangian Integrated Trajectory) back-trajectory simulations in the study area. These back-trajectories are used to highlight the origin, main pathways, and height of transported air masses during the biomass burning season (Section 3.3). The conclusions and summary are given in Section 4.

2. Location, Materials, and Method

This section is dedicated to presenting the instruments utilized in this study. We combined observations from AERONET sun photometers over several sites with satellite observations (e.g., Terra platform's MODIS (Moderate Resolution Imaging Spectroradiometer) instrument and CALIOP (Cloud Aerosol Lidar with Orthogonal Polarization) onboard CALIPSO (Cloud Aerosol Lidar Infrared Pathfinder Satellite Observations)) and the numerical tool HYSPLIT (Hybrid Single-Particle Lagrangian Integrated Trajectory) in backward mode.

2.1. Location

Eight sun photometer sites were chosen on the basis of the number of years (more than 4 years) of measurements available to cover the Southern African region and the SWIO. In Figure 1, the study sites in Southern Africa are represented by blue dots, while the Reunion site in the SWIO is represented by a red dot. The colored squares represent the location closest to each sun photometer station for MODIS observations (see Section 2.3). All geographical information is presented in Table 1.
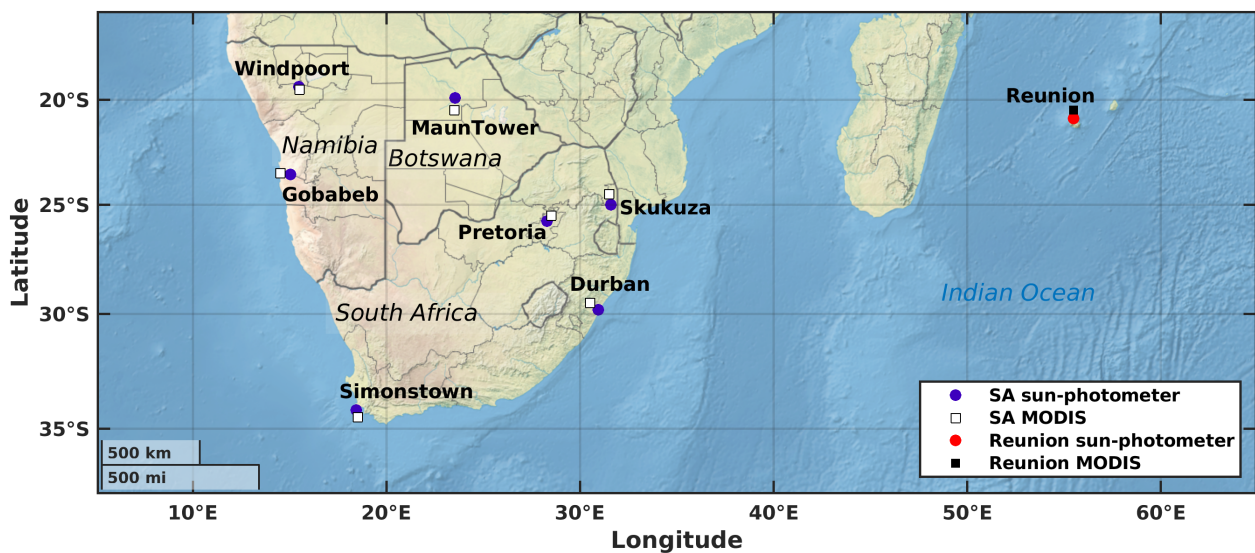

Figure 1. Geographical location of the eight sun photometer sites and of MODIS observations. The sites in South Africa (Pretoria, Skukuza, Simonstown, and Durban), Namibia (Gobabeb and Windpoort), and Botswana (Maun Tower) are identified by blue dots and white squares, and the Reunion site is shown with a red dot and a black square. Dots are for sun photometer and squares for MODIS observations.

Table 1. Geographical information of the eight sun photometer sites. Note that the site's name is shortened for readability: Reunion is known as "REUNION_ST_DENIS", Pretoria is known as "Pretoria_CSIR–DPSS", Simonstown is known as "Simontwon_IMT", and Durban is known as "Durban_UKZN". Data availability (%) is based on the ratio of the number of years available and 13 years (i.e., 2008–2021 period).

Station	Location, Country	Coordinates	Altitude (m)	Time Span, Data Availability (%)	Site Typology
Reunion	Campus of Moufia, Reunion Island	20.901°S, 55.485°E	93	2008–2021, 100	Marine
Windpoort	Etosha Pan, Namibia	19.366°S, 15.483°E	1206	2016–2021, 46.1	Rural
Gobabeb	Namib Desert, Namibia	23.562°S, 15.041°E	405	2014–2020, 53.8	Coastal, desert
Maun Tower	Botswana	19.900°S, 23.550°E	951	2017–2021, 30.7	Rural
Pretoria	Gauteng, South Africa	25.757°S, 28.280°E	1449	2011–2018, 61.5	Urban, industrial

Table 1. *Cont.*

Station	Location, Country	Coordinates	Altitude (m)	Time Span, Data Availability (%)	Site Typology
Skukuza	Mpumalanga, South Africa	24.992°S, 31.587°E	265	2008–2011 2016–2020, 69.2	Rural
Simonstown	Western Cape, South Africa	34.193°S, 18.446°E	27	2015–2021, 53.8	Urban, coastal
Durban	KwaZulu-Natal, South Africa	29.817°S, 30.944°E	205	2015–2021, 53.8	Urban, coastal

The Reunion site serves as a control region for the study of aerosol outflow from the Southern African region. The available data for the Reunion site range from the year 2008 to 2021, which corresponds to the study period for all other sites. Note that the Skukuza site data span the years from 1998 to 2020, but from 2012 to March 2016 the instrument was out of service due to calibration issues [45]. Therefore, the study period of Skukuza covers the years 2008 to 2011 and 2016 to 2020.

2.2. Ground-Based Observation from AERONET: Sun Photometer

The AERONET (AErosol RObotic NETwork) sun photometer (model CE318) is a passive remote-sensing instrument that analyzes the attenuation of solar radiation to measure the optical and microphysical properties of vertically integrated aerosols in the atmosphere (e.g., optical depth). Measurements are taken at 15 min intervals under cloud-free and daytime conditions at wavelengths of 340, 380, 440, 500, 670, 870, 940, and 1020 nm. Column water abundance is measured using the 940 nm channel. Under cloud-free conditions, the uncertainty in AOD measurements was estimated in Eck et al. [46] to be ∼0.01 in the visible and near-IR and increasing to ∼0.02 in the ultraviolet (340 and 380 nm) [46,47]. The Angström exponent (AE) is a parameter of atmospheric turbidity [48] and expresses the spectral dependence of aerosol optical depth with the wavelength; it can be estimated using AOD measurements taken at different wavelengths to provide a proxy of aerosol particle size, as given by Equation (1):

$$AE = -\frac{\ln\left(\frac{AOD_{\lambda_1}}{AOD_{\lambda_2}}\right)}{\ln\left(\frac{\lambda_1}{\lambda_2}\right)},$$

(1)

where AOD_{λ_1} and AOD_{λ_2} represent measurements at distinct wavelengths λ_1 and λ_2. AE values greater than two indicate the predominance of fine-mode aerosols, which generally correspond to biomass burning aerosols or urban pollution aerosols, whereas AE values less than unity indicate the predominance of coarse-mode aerosols, such as sea salt and dust [49]. In this study, AOD at 500 nm and the AE obtained from observations at 440 and 870 nm were used. These two parameters are referred to as AOD_p and AE in the following. The sun photometer data for the selected sites were downloaded from the AERONET website: https://aeronet.gsfc.nasa.gov/ (last accessed on 12 February 2022). The multiyear, monthly, seasonal, and annual average and median values were calculated using Level 2.0 daily data (cloud-screened and quality assured). The daily data were calculated when three or more data points were recorded.

2.3. Satellite Observations

2.3.1. MODIS Aerosol Data Set

The Moderate Resolution Imaging Spectroradiometer (MODIS) is carried onboard NASA's Aqua (EOS PM-1) and Terra (EOS AM-1) satellites, which have heliosynchronous orbits and have been operational since 2002 and 2000, respectively. MODIS collects data in 36 discrete spectral bands ranging from 0.4 to 14.4 μm, with spatial resolution varying

from 250 m to 1 km depending on the channel. MODIS products provide several quantities derived from the measure of radiance. These quantities are the distribution of cloud cover, the amount of water vapor in an atmosphere column, the distribution of temperature, and aerosol properties. The data used are the "Combined Dark Target and Deep Blue AOD at 0.55 micron for land and ocean (MOD08_D3_v6.1)", collected from the Terra platform on a 1° × 1° grid with daily temporal resolution. The Giovanni website was used to download aerosol observations (https://giovanni.gsfc.nasa.gov/giovanni/, last accessed on 7 May 2022). AOD from MODIS observations data (called AOD_{MODIS}, hereafter) were taken to the closest point to each sun photometer station (see Figure 1). For each site, the time period starts when the sun photometer becomes active and ends on 31 December 2021. Because the study period from AOD_p at Skukuza was set to begin in January 2008, we considered the same for MODIS.

2.3.2. CALIPSO Aerosol Profiles

The Cloud Aerosol Lidar with Orthogonal Polarization (CALIOP) is the primary instrument onboard the Cloud Aerosol Lidar Infrared Pathfinder Satellite Observations (CALIPSO) mission, jointly launched in April 2006 by NASA and CNES (Centre National d'Études Spatiales). It is a polar-orbiting satellite belonging to the A-Train Constellation, flying at an altitude of 705 km with a cycle of 16 days. Its aim is to study the impact of aerosols and clouds on Earth's radiation budget and climate. The CALIOP instrument is an elastic backscatter lidar operated at two wavelengths: 532 and 1064 nm. It measures the vertical distribution of aerosols and clouds, as well as their microphysical and optical properties, using two 532 nm receiver channels and a channel measuring the total 1064 nm return signal [50]. The dataset used is the Level-3 tropospheric aerosol profile product (Tropospheric_APro_V4.20 and V4.21, downloaded from the EarthData website: https://search.earthdata.nasa.gov/, last access 18 March 2022) for "cloud-free" conditions during both daytime and nighttime from 2008 to 2021; at the time of conducting this work, data were available until October 2021.

The advantage of this dataset is that it corresponds to a combination of quality-screened Level-2 aerosol data and includes aerosol extinction profiles at 532 nm as well as layer classification information (i.e., aerosol, cloud, and "clear air"—meaning air without aerosols). The CALIOP Level-3 aerosol profile product is based on monthly statistics, with all Level-2 aerosol profiles reported separately each month at a near-global scale (180°W to 180°E, 85°N to 85°S) on a uniform 2.0° × 5.0° (latitude × longitude) grid box with a vertical resolution of 60.0 m from 0.5 to 12.0 km (total of 208 layers) above mean sea level. Data were selected on a latitude × longitude grid box of 2.0° × 5.0° to obtain the vertical distribution of each aerosol type for each site. Each collection grid is shown in Figure A1, Appendix A. Due to CALIOP L3 data resolution, Skukuza and Pretoria were merged into a larger grid box. According to Gui et al. [51], the South Atlantic Anomaly degrades the quality of the Level 3 data in 2017 and 2019. As a consequence, there are no data for these three years at Windpoort and Gobabeb.

2.4. HYSPLIT Back-Trajectories

The HYSPLIT (Hybrid Single-Particle Lagrangian Integrated Trajectory) model was developed by NOAA and ARL [52]. This model calculates simple air parcel trajectories as well as complex gaseous or particulate pollutants' transport, dispersion, chemical transformation, and deposition. The calculation method is a hybrid that combines the Lagrangian and Eulerian approaches, using meteorological fields such as wind components, temperature, and humidity from archived reanalyses. In this study, the Global Data Assimilation System (GDAS) meteorological fields were used. GDAS data have a horizontal resolution of 1° × 1°. We used the backward mode of the HYSPLIT model to determine the origin of the aerosol particles observed during the spring season, which coincides with the biomass burning season in Southern Africa. Based on the results of the vertical distribution of aerosol type obtained with CALIOP, we chose 9 height levels ranging from 2 to 6 km with a

resolution of 500 m. To cover the biomass burning season, we ran simulations of 120 h per height every 10 days from 2008 to 2021 between August and November. As mentioned by Hernández-Ceballos et al. [53], 120 h is considered sufficient to represent synoptic air flows. There are 9 simulations per height level and 13 per year for a total of 1638 simulations per site. The simulation results were then clustered and analyzed for each site to determine the origin of the aerosol particles observed during biomass burning seasons. We clustered the trajectories using TrajStat, an algorithm developed by Wang et al. [54] as a GIS-based program to view, query, and group the trajectories. This program had already been used in the study of Millet et al. [55] in the identification and analysis of the observed seasonal aerosol variations over Southern Morocco. The number of clusters can be visually determined by inspecting the total spatial variation (TSV) curve before a net increase in TSV (see Figure A2, in Appendix A).

2.5. Methodology

Normally, a scatter plot between the AOD_p and the AE is used to classify different aerosol types over a study site. This method has been widely used in a number of studies [37,38,56] and over South Africa [19,22,23]. Due to the greater availability of AOD and AE values rather than daily averages of single-scattering albedo, fine-mode fraction, absorption Angström exponent, and extinction Angström exponent (SSA, FMF, AAE, and EAE, respectively), this relationship is preferred over others, such as SSA vs. FMF [23,26] or AAE vs. EAE [57–59]. The selection of threshold values to distinguish the type of aerosol is very important and varies based on geographical location [60].

In this present study, we used the classification threshold values presented by Kumar et al. [19] over Skukuza, in South Africa. These values are summarized in Table 2. The plot based on this method is shown in Figure 2. For the purpose of naming the aerosol clusters, aerosols were categorized as clean marine (CM), biomass burning and urban industrial (BB/UR), and desert dust (DD). The aerosols that do not fit into any of the above categories/clusters are classified as mixed (MX) aerosols. The use of the term "mix" for these mixed aerosols arises from the result of mixing between particles of different sizes that belong to variable sources.
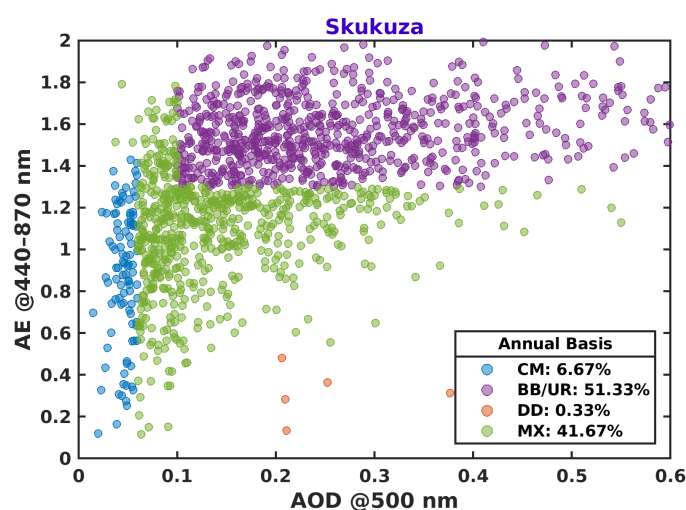

Figure 2. Diagram of aerosol classification at Skukuza (2008–2011 and 2016–2020) defined by using threshold values from Kumar et al. [19]. Each color is associated with an aerosol type: clean marine (CM, in blue), biomass burning/urban industrial (BB/UR, in purple), desert dust (DD, in orange), and mixed type (MX, in green). The frequencies of occurrence for each type account for the annual basis.

Table 2. Threshold values of aerosol optical parameters to classify aerosol types over study sites.

Aerosol Type	AOD	AE
clean marine (CM)	AOD < 0.06	AE < 1.5
desert dust (DD)	AOD > 0.15	AE < 0.5
mixed (MX)	-	-
biomass burning and urban industrial (BB/UR)	AOD > 0.1	AE > 1.3

We used this aerosol classification method for the eight study sites in order to determine the occurrence frequency of each aerosol type on a seasonal and annual basis. All values of the occurrence frequency are presented in Section 3.1.4 in figure. For a given site and aerosol type, the relative frequency of occurrence for each season, as a percentage, is defined by Equation (2):

$$FQ_s(\text{type}) = 100 \times \frac{N_s(\text{type})}{N_s},\qquad(2)$$

where $N_s(type)$ is the number of occurrences for a given aerosol type and season, and N_s is the total number of occurrences for the given season (for all types).

The multiyear annual relative frequency of occurrence, as a percentage, for a given site is defined as in Equation (3):

$$FQ(\text{type}) = 100 \times \frac{\sum N_s(\text{type})}{N},\qquad(3)$$

where $\sum N_s(type)$ is the sum of the number of occurrences of each season for a given aerosol type and N is the total number of occurrences.

The aerosol subtyping algorithm considers seven aerosol types for each height level based on lidar and depolarization ratios [61]. They are defined as clean marine (sea salt), dust (desert), clean continental (clean background), polluted continental/smoke (urban/industrial pollution), elevated smoke (biomass burning aerosol), polluted dust (dust mixed with anthropogenic aerosols such as biomass burning smoke or urban pollution), and dusty marine (mixtures of dust and marine aerosols near the ocean surface).

The frequency of occurrence, in percent, of each aerosol type from CALIOP observations at different heights is defined using Equation (4), the same as in Gui et al. [51]:

$$FO_{CALIOP} = \frac{N_{aerosol}}{N_{total}} \times 100.0,\qquad(4)$$

where $N_{aerosol}$ represents the number of samples detected by CALIOP for a specific aerosol type at the specified height level and N_{total} is the total number of samples (including all aerosol types and "clean air") at the specified height level.

Hereafter, the seasons are defined as summer (from December to February, DJF); autumn (from March to May, MAM); winter (from June to August, JJA); and spring (from September to November, SON).

In order to compare the evolution of AOD_p with that of AOD_{MODIS}, the wavelength of the AOD_p was changed from 500 to 550 nm using the AE obtained from the sun photometer between 440 and 870 nm in Equation (1) [21,62,63]. The statistical parameters used for the comparison are the correlation coefficient (r), root mean square error (RMSE), and mean bias error (MBE), whose formulas are as follows:

$$r = \frac{\sum_{i=1}^{N}(AOD_{p_i} - \overline{AOD_{p_i}})(AOD_{MODIS_i} - \overline{AOD_{MODIS_i}})}{\sqrt{\sum_{i=1}^{N}(AOD_{p_i} - \overline{AOD_{p_i}})^2 \sum_{i=1}^{N}(AOD_{MODIS_i} - \overline{AOD_{MODIS_i}})^2}}\qquad(5)$$

$$RMSE = \sqrt{\frac{1}{N} \sum_{i=1}^{N} (AOD_{p_i} - AOD_{MODIS_i})^2}, \tag{6}$$

$$MBE = \frac{1}{N} \sum_{i=1}^{N} \frac{AOD_{p_i} - AOD_{MODIS_i}}{AOD_{p_i}}, \tag{7}$$

where N represents the total number of samples (AOD values) and the overbar indicates the average of all N values.

The statistical parameters shown above have also been used in several similar studies where ground-based and satellite observations were compared [55,63,64]. The RMSE is normally used to calculate the difference between expected and observed values—in this case, between MODIS observations and sun photometer measurements. The systemic bias between two time series is calculated using the MBE, where a negative MBE value shows the satellite overestimation of one time series by the other. In addition, a linear regression analysis was conducted between the two datasets and is reported in Section 3.1.3 in figure.

3. Results

3.1. Spatiotemporal Evolution of Aerosol Optical Properties and Aerosol Types

3.1.1. Monthly Evolution

Figure 3 shows the time series of the monthly average and ±1 standard deviation value of AOD at 550 nm from sun photometer and MODIS observations at eight sites from 2008 to 2021. For ease of reading and comparison, the figures in this part are organized by the latitude and longitude of sun photometer sites.

Based on the 13-year period (2008–2021), Skukuza, Pretoria, and Reunion have the longest time series (corresponding to 69.2, 61.5, and 100% of data availability, see Table 1). Simonstown, Gobabeb, and Durban present time series with 53.8% of data availability for seven years of measurements. Windpoort and Maun Tower show shortened time series with 46.1 and 30.7% of data availability and more than four years of measurements. Despite the difference in the length of the sun photometer dataset, time series analysis reveals an annual variation that coincides with the maxima during the spring season. This season corresponds to the biomass burning season, which lasts from August to November in Southern Africa. In September, AOD peaks exceed 0.4 in Windpoort, Maun Tower, Skukuza, Pretoria, and Durban.

As mentioned in the methodology section, MODIS data were taken closest to each AERONET station and only time-coincident measurements were considered.

For both instruments (sun photometer and MODIS), the lowest and highest annual average AOD values are found in Simonstown (0.07 ± 0.02 and 0.12 ± 0.02) and Skukuza (0.19 ± 0.09 and 0.15 ± 0.05), respectively. Both Reunion and Simonstown have similar AOD evolution, with a low multiyear annual average value of 0.07.

Similarly to with AOD, the time series of AE are in Figure 4 to give an idea of the predominant aerosol mode from sun photometers. The AE time series in Pretoria show the highest values, around 1.5 throughout the year with an average of 1.52. For Maun Tower, Windpoort, Durban, and Skukuza AE time series, the average varies between 1 and 1.5. The AE time series show values from 0.5 to 1 for Simonstown and Reunion and from 0.5 up to 1.5 for Gobabeb. One can note that even though Durban is a coastal site, AE values reach 1 to 1.5, such as in Pretoria. This illustrates the urban nature of the Durban site.
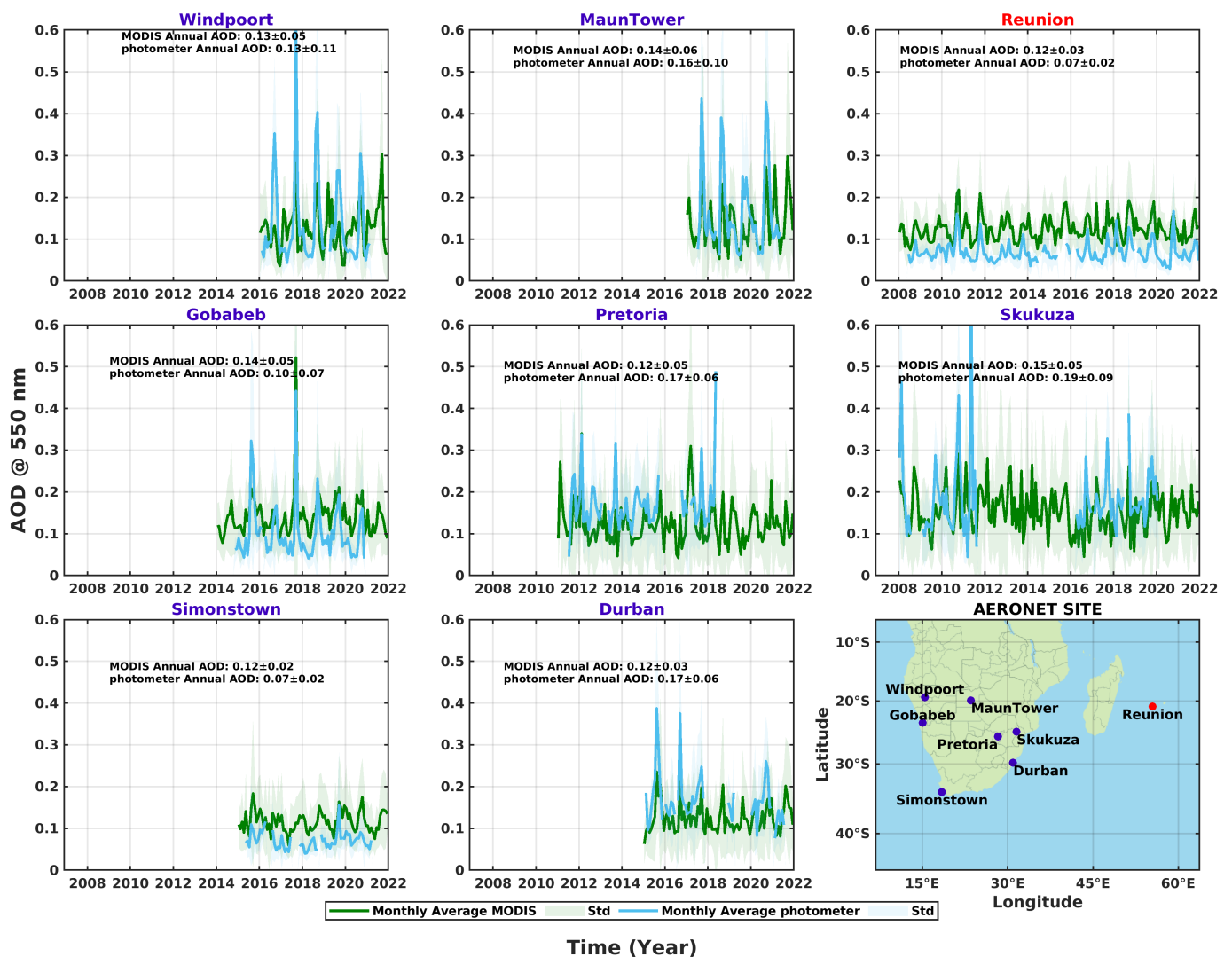
Figure 3. Time series of AOD at 550 nm over the eight sun photometer sites. Solid lines (shaded area) show monthly average (±1 standard deviation) from the sun photometer in blue and from MODIS observations in green. Multiyear annual AOD values for both instruments are provided during the study period. The bottom right panel represents the location of sun photometer sites.

With regard to the annual multiyear average values, they are greater than unity for all sites, indicating that fine-mode particles predominate. Simonstown and Reunion exhibit values lower than unity, indicating that coarse-mode particles are predominant over these sites.

The average annual multiyear AOD and AE values supported by this finding are of similar magnitude to those observed in previous works (see Table A1 in Appendix A, which summarizes our results and places them in a broader context of aerosol optical properties published in the literature for Southern Africa). Based on previous work, the most studied sites in the last decades are Skukuza and Pretoria, followed by Cape Town, Durban, and Reunion Island. Other study locations, such as Windpoort, are only used for brief periods of time during measurement campaigns (such as during the AEROCLO-sA field campaign [17]). The slight difference in the multiyear average values of AOD and AE compared with these previous works can be due to different periods, the shift in wavelength, and the different datasets, particularly for MODIS observations.
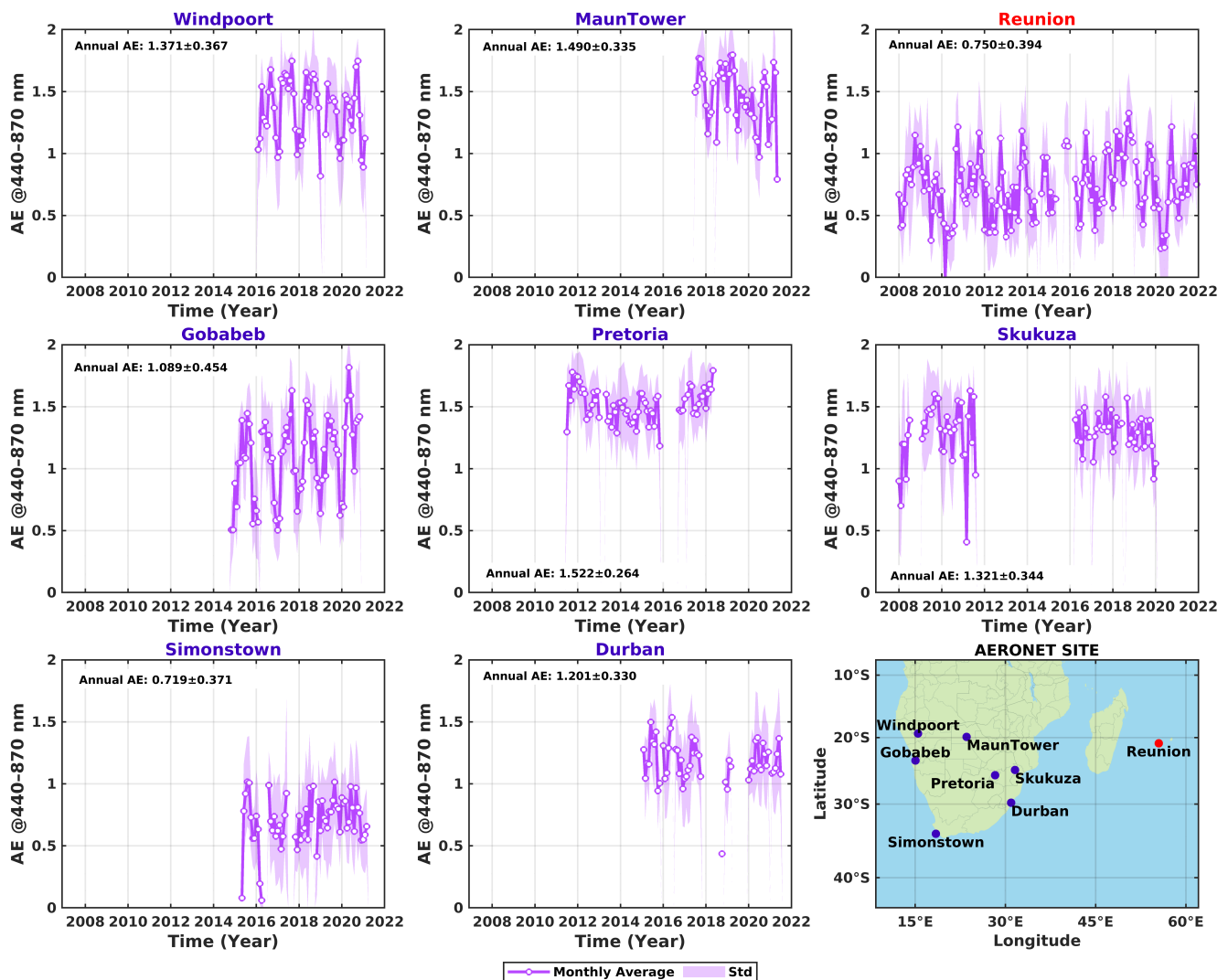
Figure 4. Time series of AE at 440–870 nm over the eight sun photometer sites. Solid lines (shaded area) show monthly average (±1 standard deviation). Annual AE values are provided during the study period. The bottom right panel represents the location of sun photometer sites.

3.1.2. Seasonal Evolution

In Figure 5, the seasonal variations in AOD_p, AOD_{MODIS}, and AE are represented by box plots in blue, green, and purple, respectively.

During the spring season, AOD_p values are highest, with mean values ranging from 0.09 at Reunion to 0.22–0.24 at Windpoort, Durban, Maun Tower, and Skukuza. AOD_p values at Simonstown are higher during the winter season, with a mean of 0.07. The winter season accounts for the lowest average AOD_p values, which range from 0.05 at Reunion to 0.13–0.15 in Pretoria and Skukuza. During the autumn season, the average AOD_p values range from 0.06–0.07 (Simonstown, Gobabeb, and Windpoort) to 0.1. (Maun Tower). In contrast to AOD_p, AE levels are higher in the spring, although only at a few sites. The mean value ranges from 0.09 at Reunion to 1.4–1.5 at Gobabeb, Windpoort, Maun Tower, and Skukuza. AE values are higher during the winter season at Simonstown and Durban, with mean values of 0.07 and 1.19, respectively. Finally, AE values in Windpoort and Pretoria are greater in the fall season, with mean values of 1.47 and 1.51, respectively. The winter season has mean values ranging from 0.6 (Reunion) to 1.3–1.4 (Maun Tower and Pretoria), while the summer season has mean values ranging from 0.6–0.9 (Windpoort and

Gobabeb) to 1.44–1.47 (Maun Tower, Pretoria, Skukuza, and Durban). Finally, the autumn season has an average value of 0.4 in Simonstown.
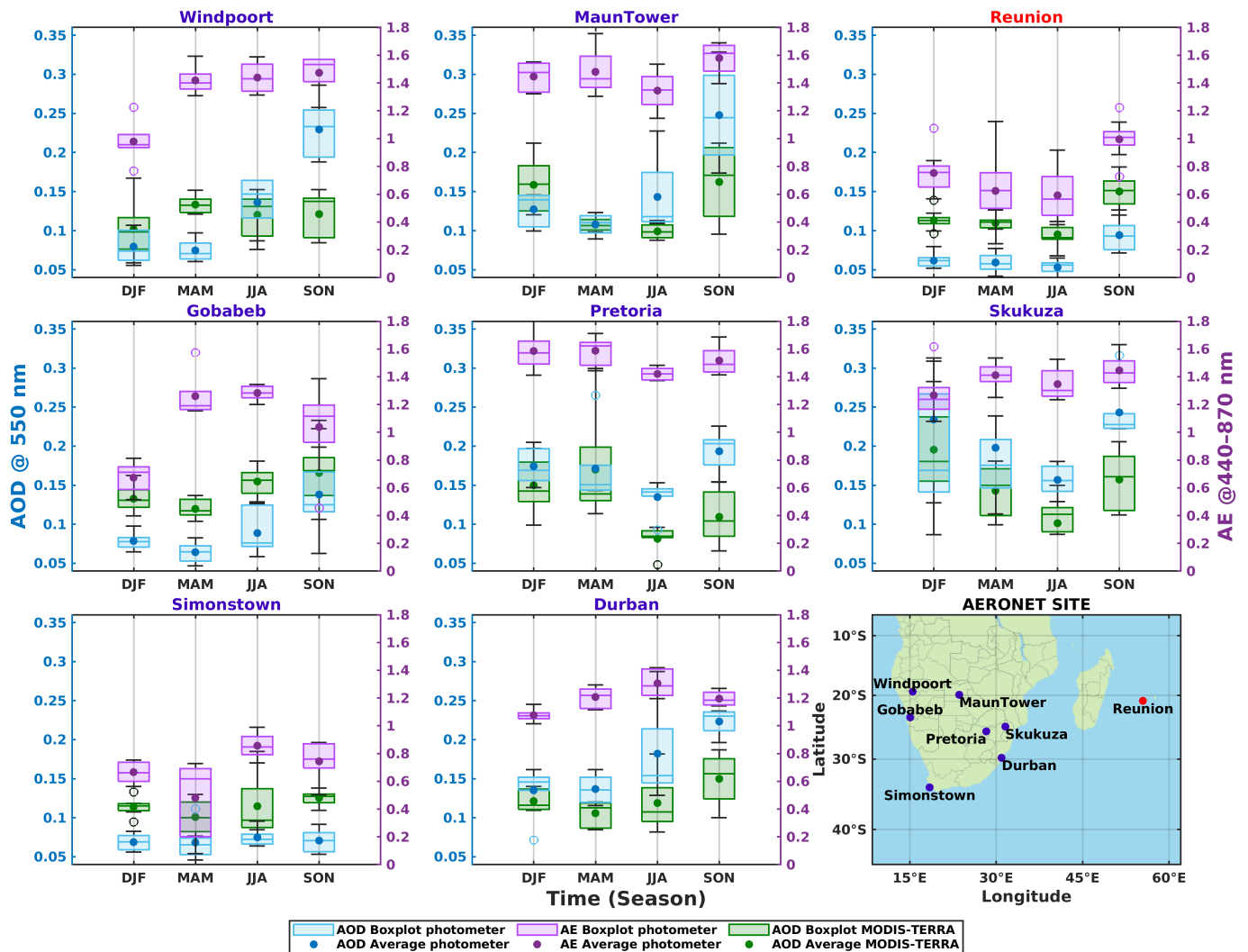

Figure 5. Multiyear seasonal average (±1 standard deviation) of AOD at 550 nm (blue for sun photometer and green for MODIS observations) on the left vertical axis and AE at 440–870 nm (purple) on the right vertical axis over the eight sun photometer sites. The colored box diagrams for each season are December to February (DJF), March to May (MAM), June to August (JJA), and September to November (SON). The median is the central value (the line inside the boxes). The edges of the boxes are set at the 25th and 75th percentiles. The whiskers show the extreme values, excluding outliers, which are represented by shaded colored circles. Filled colored dots indicate average values.

Unlike the AOD with sun photometers, the AOD_{MODIS} is only high in the spring season at Reunion, Maun Tower, Gobabeb, Simonstown, and Durban, with AOD average values ranging between 0.12 and 0.16. The autumn season at Windpoort and Pretoria has the highest values, with average values of 0.13 and 0.14. Finally, Skukuza has higher values in the summer, averaging 0.19. During the winter season, the AOD_{MODIS} values range from 0.08–0.09 (Pretoria, Maun Tower, and Reunion) to 0.10 (Skukuza), and in autumn, they are about 0.10–0.11 (Gobabeb, Simonstown, and Durban). Finally, throughout the summer, the AE values in Windpoort are low, with an average of 0.10.

The highest values being during spring could be due to the passage of smoke plumes over the sites. On the one hand, certain locations have AE values larger than unity through-

out the year—notably, urban/industrial sites such as Durban and Pretoria, and rural sites such as Skukuza, Maun Tower, and Windpoort.

This may be due to high levels of pollution caused by the combustion of fossil fuels (traffic and industry). On the other hand, coastal sites have AE values below unity for all seasons except spring, with the exception of Durban, which is both an urban and coastal site, and its AE values are more than unity in all seasons. This emphasizes the impact of biomass burning in the spring as well as the background aerosol environment of these sites during the other seasons.

3.1.3. Intercomparison

For the purpose of this study, the relationship between sun photometer and MODIS observations is investigated. Figure 6 shows the scatter plot that depicts the intercomparison between daily data from sun photometer and MODIS observations over the same time period for each dataset and each site. The statistical parameters summarized in each panel of the figure were calculated using Equations (5)–(7) and are reported in Figure 6. In general, the correlation coefficient (r) ranges between 0.50 to 0.78, with lower values over coastal/maritime sites (e.g., Reunion, Gobabeb, and Simonstown) and the inland site Windpoort. Higher correlation coefficient values are reported over rural or urban sites such as Durban, Maun Tower, Pretoria, and Skukuza. Maun Tower and Durban have the highest correlation coefficients of 0.78 and 0.76, respectively. It is important to note that in a coastal site such as Durban, which reported a high correlation of 0.76, both sensors are expected to detect marine and urban aerosols. In addition, this site is also expected to be affected by seasonal sugarcane burning activity that takes place in nearby sugarcane farms [65].

There seems to be a possible difference between the sensing capability of the ground-based instrument and satellite sensors in different coastal regions that could be associated with the different meteorological and dynamical conditions between the east and west coasts of Southern Africa. Furthermore, the results presented in this study are similar to other studies that compared satellite data and sun photometer observations of AOD over South African and reported correlation coefficient values ranging from 0.70 to 0.78 [21,25,63]. Coastal sites, with the exception of Gobabeb, experience lower RMSE values of 6.46%, 6.66%, and 8.85% for Simonstown, Reunion, and Durban, respectively. The highest RMSE values of 11.11% and 12.49% were reported at the Gobabeb and Windpoort sites, respectively. The lowest correlation coefficient values were also reported for these two sites, which have a stronger spread of data points in the scatter plot, indicating differences between the sun photometer and satellite sensor AOD values in some cases. Gobabeb and Windpoort are located closer to the Namib Desert and are thus expected to experience a high desert dust load. The results presented in this study seem to indicate an overestimation of AOD by MODIS with respect to sun photometers, which is consistent with the results presented by Tripathi et al. [66]. In addition, negative values of MBE are found over Reunion (MBE = −4.90%), Simonstown (MBE = −3.92%), and Gobabeb (MBE = −5.17%); this is also indicative of an overestimation of AOD from MODIS observations.

In general, several potential causes (surface reflectance, cloud contamination, and retrieval bias) could contribute to the discrepancies between MODIS and sun photometer observations. These biases over some of the study sites may be explained by the fact that sun photometer measurements are made under cloud-free conditions at a given point, whereas MODIS is able to detect aerosols under cloudy conditions with a resolution of $1° \times 1°$. Slight contamination cannot be excluded based on the spatial resolution of the MODIS observation. A study by Hoelzemann et al. [67] showed that even minor cloud contamination can incorrectly increase the value retrieved for AOD. The AOD values from MODIS observations are slightly lower than for ground-based measurements in the regions impacted by biomass burning (Maun Tower, Pretoria, Skukuza, and Durban). This is consistent with the study by Hao et al. [68] during the SAFARI-2000 field campaign. Hao et al. [68] suggested that this discrepancy may be due to an error in the assumed aerosol scattering function or surface directional properties. Conversely, the AOD val-

ues from MODIS are higher compared with sun photometer observations near and in coastal sites (Simonstown, Reunion, and Gobabeb). This is consistent with previous work, which found a great correlation between land sites and coastal sites due to low surface reflectance [21,25,67,69,70]. According to Madry et al. [71], the bias with coastal sites can be attributed to the generation of sea salt particles from near-surface high winds that occur along the coast.
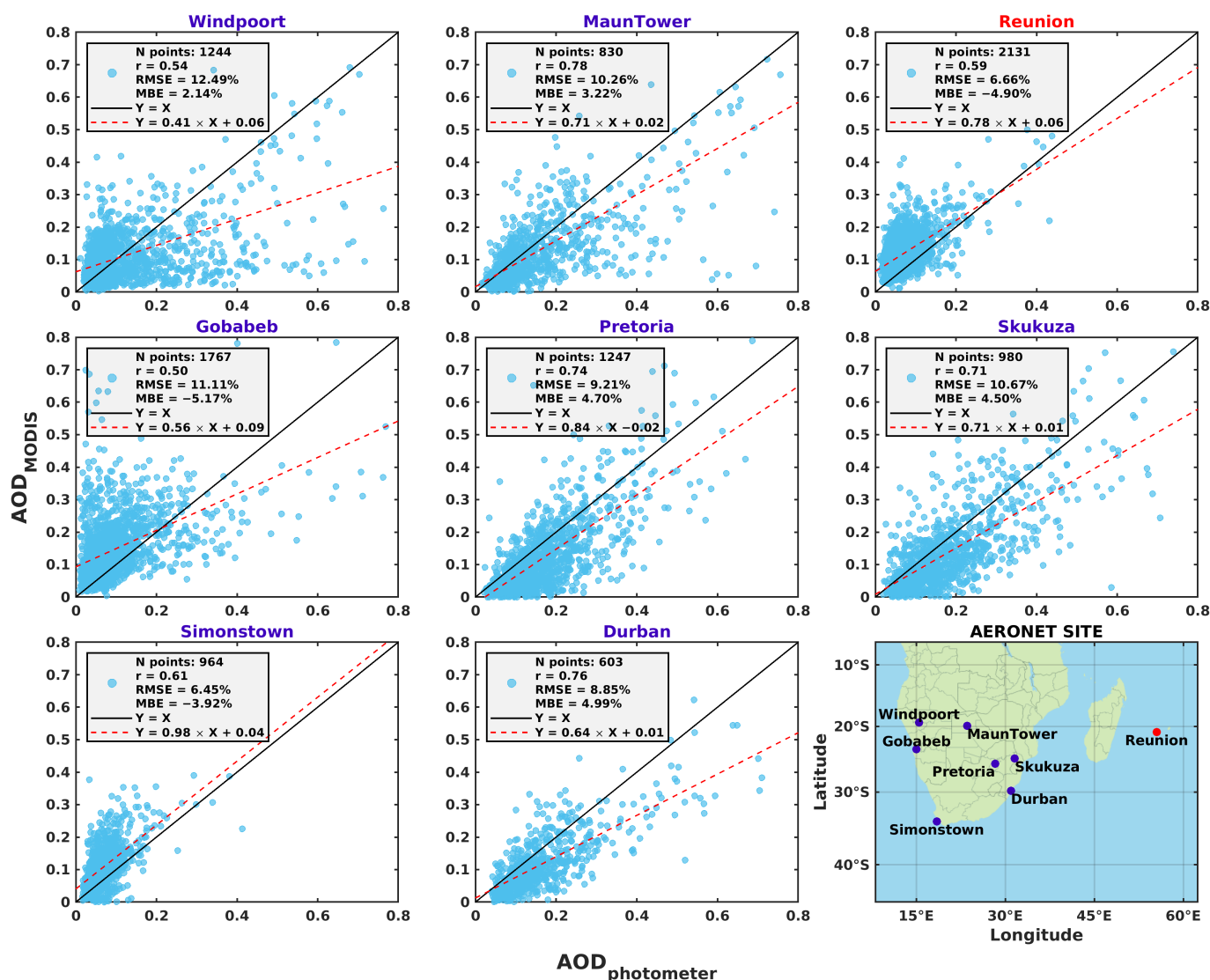

Figure 6. Scatter plot of AOD at 550 nm over the eight sun photometer sites. The total number of observations (N) for both instruments provided during the study period as well as the correlation coefficient (r), root mean square error (RMSE), mean bias error (MBE), and fitting curve (red lines). The black lines represent the 1:1 line. The bottom right panel represents the location of sun photometer sites.

3.1.4. Aerosol Type

Figure 7 presents the multiyear seasonal and annual relative occurrence frequencies of the four major aerosol types over each site.

The BB/UR type is prevalent throughout the winter and dominates in spring for sites near biomass burning areas, with values ranging from 40 to either 65% or 70%, respectively. Lower values (6–40%) are found at the remaining sites where the MX type predominates. The increases in BB/UR frequencies observed during the spring are caused by biomass burning, which mostly affects sites near biomass fire sources. However, some sites, such

as Pretoria, Durban, and Skukuza, have consistently high BB/UR frequencies throughout the year. This highlights the nature of each site: industrial for Pretoria, urban for both Pretoria and Durban, and rural for Skukuza. Conversely, Simonstown and Reunion are far away from the biomass burning areas, with very low BB/UR frequencies and high CM and MX frequencies. CM values are highest in the autumn, when the trade winds are at their maximum. Compared with these two coastal and maritime sites, Durban, which is also a coastal site, has lower CM values. In general, these abovementioned findings seem to highlight the influence of the geographical context of each station.
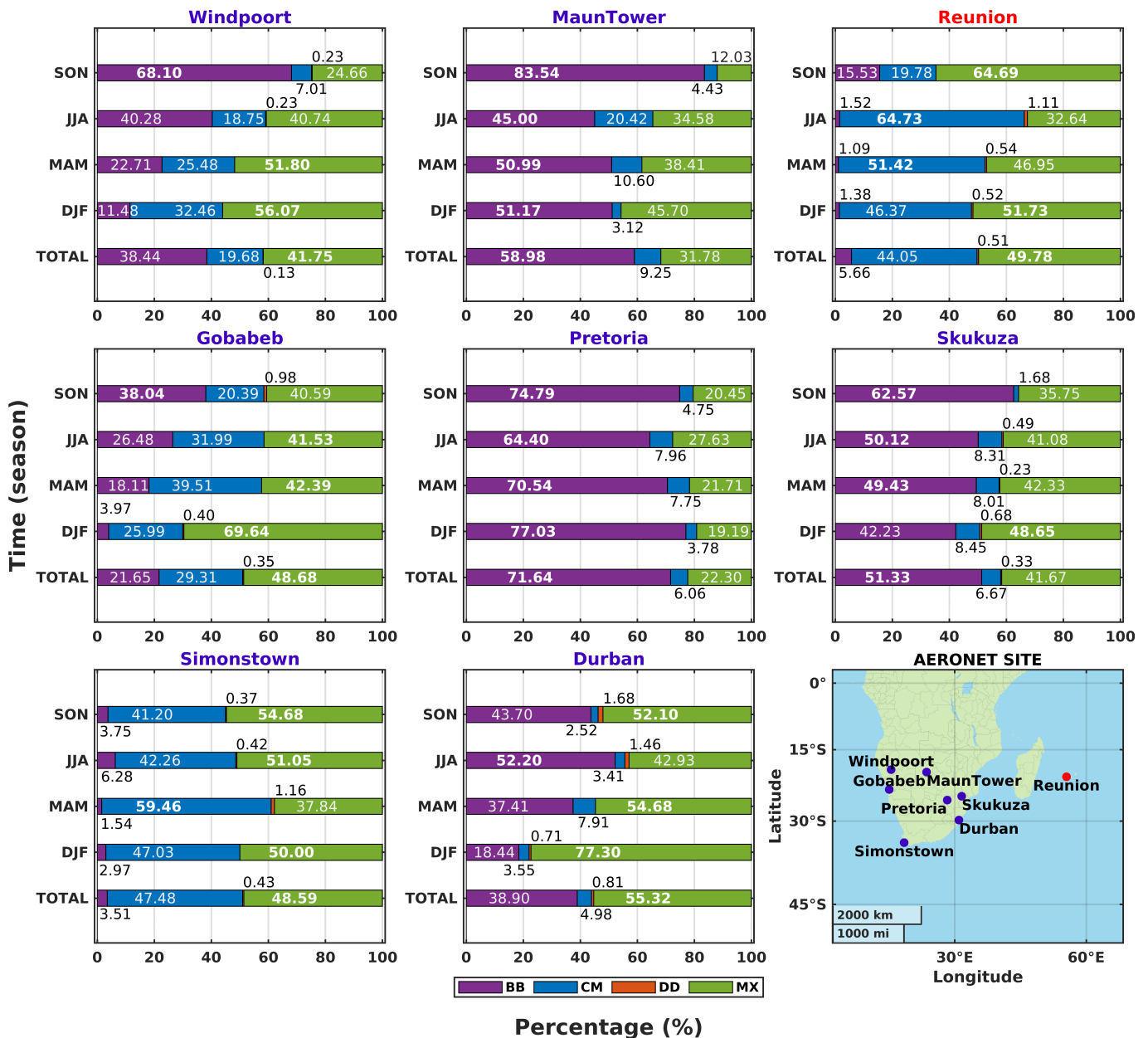

Figure 7. Aerosol classification from sun photometer data over the eight sun photometer sites. The multiyear seasonal and annual (referred to as "TOTAL") relative occurrence frequency as a percentage. Each type is associated with one color: clean marine (CM) in blue, biomass burning/urban industrial (BB/UR) in purple, desert dust (DD) in orange, and mixed type (MX) in green.

Examining the aerosol optical properties and aerosol types reveals the highest AOD values and highest frequencies of the BB/UR aerosol type for some sites in spring and summer.

The investigation of aerosol type based on the relationship between AOD and AE allows obtaining a preliminary idea of the major aerosol types. However, this approach and the associated threshold values do not allow for the distinction between biomass burning and urban/industrial aerosol types. This is due, in part, to the threshold values established for urban and semi-urban locations, where industrial activity and local air pollution dominate the background (e.g., Durban, Pretoria, and Skukuza). As a result, the pair (AOD > 1 and AE > 1.3) suggests moderate to high turbidity conditions under the impact of a mixed aerosol field with a higher proportion of local urban industrial aerosols and transported biomass combustion aerosols. Furthermore, dust aerosol can be masked, as seen over Gobabeb in the Namibian Desert, which has lower dust frequencies. Dust aerosols appear more frequently in mixed mode and undergo changes during their transport from the source to sun photometer, and are hence not classified as DD aerosols [30]. The relative seasonal contribution of each aerosol type is highly dependent on the synoptically changing source and sink strengths, the transport component and its pathways, local meteorology, and the mixing processes in the atmospheric column.

As a result, the CALIOP observations and the back-trajectory model will support the first part. In the following subsection, CALIOP profiles are used to analyze the vertical aerosol type distributions over each study site.

3.2. Vertical Distribution with CALIOP

Figure 8a depicts the average occurrence frequency profiles of each aerosol type for each of the eight sites, as derived from CALIOP measurements from 2008 to 2021. In general, the major aerosol types with occurrence frequencies above 10% are polluted continental/smoke (orange line), polluted dust (brown line), and elevated smoke (black line), while dust (yellow line), clean continental (green line), and dusty marine (sky-blue line) are minor aerosol types with occurrence frequencies below 1%. Clean marine (dark-blue line) and dusty marine types are present in the planetary boundary layer (PBL), with occurrence frequencies close to 80 to 85% and 10 to 15%, respectively. Because occurrence frequencies above 6 km tend to be low (lower than 1%), all of the profiles in this figure are limited to 8 km. Occurrence frequencies above this range may match the study case but are not relevant to the aim of this article. Note here that Skukuza and Pretoria are grouped together due to CALIOP L3 data resolution (2.0° × 5.0°).

The advantage of CALIOP is that it distinguishes between urban/industrial pollution and biomass burning aerosol types, which are referred to as polluted continental/smoke and elevated smoke, respectively. Given our interest in biomass burning aerosols, we examined the vertical distribution of the elevated smoke for each season, with results shown in Figure 8b.

It is worth noting that the vertical profiles of elevated smoke exhibit different shapes in spring in comparison with other seasons. There is a seasonal shift in the peak altitude where elevated smoke is encountered. In fact, we generally observe a significantly enhanced altitude during the spring season, when fire activity is at its maximum. This increase is significantly more pronounced (with a shift greater than 1 km) for sites nearest to biomass burning areas (such as Maun Tower, Windpoort, Skukuza, and Pretoria).

From Figure 8b and by regrouping sites into three regions (north, west coast, and east coast), we note the following:

- The northern regions (Windpoort, Maun Tower, and Reunion) present the same elevated smoke profiles around 3–4 km with occurrence frequencies at 32% on average (at Windpoort and Maun Tower, 26.7% and 39.2%, respectively). The Reunion site (found at the same latitude) presents lower values of occurrence frequencies, with a maximum of 8.8% at 2.7 km.
- The west coast (Gobabeb and Simonstown) has the highest altitude peak in occurrence frequency, at 4.5 km (13.6%), particularly at Gobabeb. We note that Simonstown presents very low values of occurrence frequencies, where the maximum is 1.1% at 3.9 km.

- The east coast (Skukuza and Pretoria (which are grouped in the same box) and Durban) has its maximum occurrence frequency (17.1%) at 3.3 km, while Durban remains low at 2.7 km (8.7%).
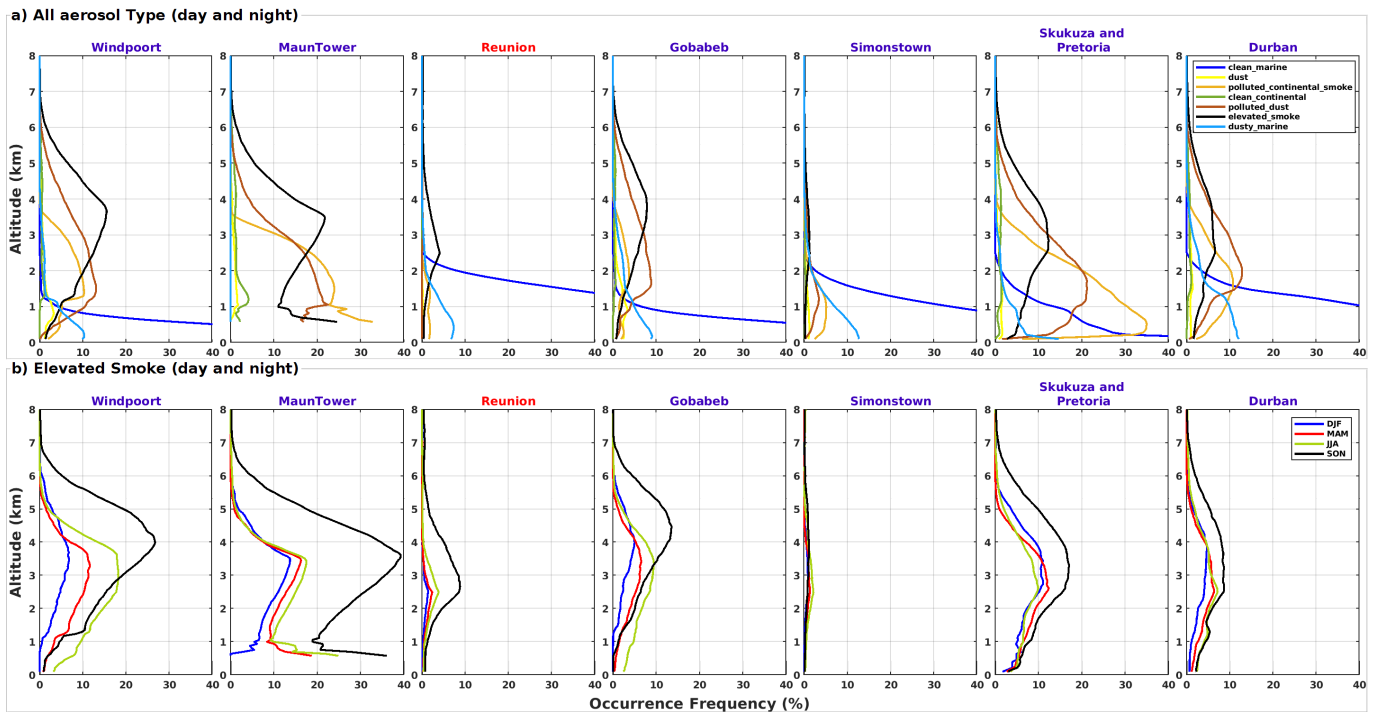

Figure 8. Vertical distribution of occurrence frequencies of aerosol types from CALIOP over the eight sun photometer sites. (**a**) Multiyear average annual values of all aerosol types: clean marine (dark-blue line); dust (yellow line); polluted continental/smoke (orange line); clean continental (green line); polluted dust (brown line); elevated smoke (black line); and dusty marine (sky-blue line). (**b**) Multiyear seasonal average values of elevated smoke: summer (DJF, dark-blue line), autumn (MAM, red line), winter (JJA, light-green line), and spring (SON, black line).

However, one should be cautious in interpreting these results since the CALIOP aerosol type algorithm is limited in identifying smoke layers. The air masses lofted by convective processes or other vertical transport mechanisms can be misclassified as elevated smoke [61]. Another limitation with CALIOP is the resolution grid ($2.0° \times 5.0°$), which is very coarse and may thus bias the results for some sites. For example:

- At Maun Tower, vertical profiles do not begin at the surface such as with the other sites (Figure 8); this is probably due to considering an average of the topography. It is worth mentioning that the two peaks of elevated smoke could be attributed to being in proximity to a biomass burning region.
- Skukuza and Pretoria sites are both close to biomass burning sources, such as Maun Tower or Windpoort, but present lower occurrence frequency of elevated smoke. It should be noted that Pretoria is more urbanized and industrialized than Skukuza. Figure 8a shows that polluted continental occurrence frequencies are higher than those of elevated smoke.

Despite these limitations in classifying aerosol types by the use of sun photometer and CALIOP observations, the two methods of aerosol classification complement each other. Higher frequencies of elevated smoke and BB/UR aerosols are found for sites that are close to biomass burning areas, while lower frequency values are found for sites away from sources. Those sites may be more influenced by biomass burning via transport mechanisms. The following subsection investigates air mass transport in order to identify the potential origin of air masses that may impact aerosol load over the study region.

3.3. Identification of Potential Origin of Air Masses

Figure 9 shows the clustered back-trajectories from HYSPLIT made for the eight sites in the 2–6 km altitude ranges from August to November over the 2008–2021 period. It is clear that the majority of the clustered trajectories correspond to intercontinental transport with air masses passing across South America and the Atlantic Ocean. There is regional transport with air masses coming from Southern Africa and locally recirculating around the sites. The height of transportation levels varies along each cluster from 1 to 8 km, with the top altitude reaching 8 km above the Atlantic Ocean. The details of height level of each back-trajectory cluster are proposed in the Appendix A, Figure A3.

As established in the previous subsection, sites are grouped into three regions (north, west coast, and east coast). Regions are referred to as panels (a), (b), and (c), where panel (c) is subdivided in three panels (c1), (c2), and (c3).

Windpoort, Maun Tower, and Reunion, which correspond to northern regions, are in Figure 9a. Due to the similarity of air mass pathways and because latitude is nearly the same for Reunion as for the first two sites, the Reunion site is included in panel (a). The clustering analysis applied to HYSPLIT back-trajectories reveal five clusters for Maun Tower and three clusters for both Windpoort and Reunion sites. The majority of air masses transported at Windpoort and Maun Tower originated in the Atlantic Ocean, near the west coast of Southern Africa (from 8 to 50%), and then in the east part of Southern Africa, which corresponds rather well to local recirculation (from 20 to 33%). Then, the back-trajectories of South America culminate at a height of 8 km before arriving in Southern Africa. Concerning Reunion, the majority of back-trajectories originate in South Africa's North West province (50%); then in the east over the Indian Ocean; and, finally, with a smaller percentage (18%), from the Atlantic Ocean.

Figure 9b includes Gobabeb and Simonstown, both on Southern Africa's west coast. Five back-trajectory clusters were obtained for Simonstown and three for Gobabeb. At Gobabeb, 46% of air mass transport occurs over Namibia, with the remaining clusters arriving from the Atlantic Ocean and South America. All of the clusters for Simonstown occurred over the Atlantic and from South America.

Figure 9c1–c3 depict maps of cluster analyses applied to back-trajectories obtained over Skukuza, Pretoria, and Durban, respectively. These three sites are relatively close and located on the east coast of Southern Africa. They are separated due to their large number of clusters. Four back-trajectory clusters were obtained for both Pretoria and Durban, and five for Skukuza. The sites present similar trajectories, with similar percentages at Durban and Pretoria. The cluster back-trajectories travel across Namibia from South America and the Atlantic Ocean (accounting for 13 to 46%). The crossing over cluster back-trajectories from Durban takes place further south, near the Northern and Western Cape provinces. Finally, all three sites have recirculation of air masses (accounting for 13 to 23%).

In previous works, a single day from August to November was used to characterize a season, with an arrival height of below or around 3000 m [18,20–22,24,27,30,72]. Then, Kumar et al. [21,22] present clustered trajectories over several years for the spring season in Pretoria and Durban. Even though the methods differ, the clustering back-trajectories in Figure 9 are consistent with those in previous works on Southern Africa. However, because we used several sites and a longer period to characterize the biomass burning season, our results are more up to date.

During the spring season, local biomass burning and long-range transport influence Southern Africa's air flows and modulate AOD over the region. The results for back-trajectories presented here depict common trajectories of tropospheric circulation over Southern Africa, which was also established by Garstang et al. [7], even though they only provide the origin and transport of air masses.
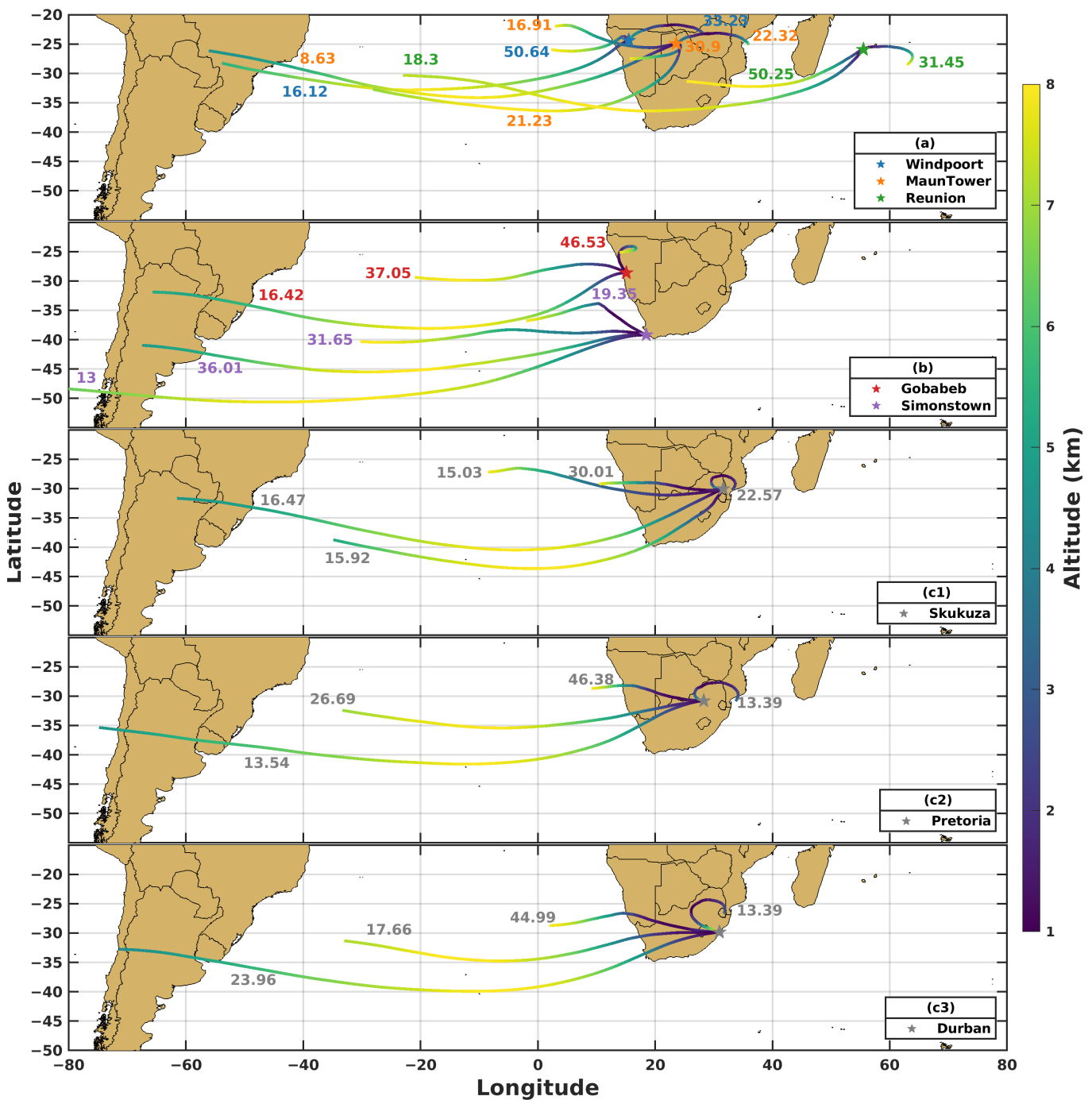
Figure 9. Map of clustered back-trajectories as simulated by the HYSPLIT model between August 2008 and November 2021, with air masses ending between 2 and 6 km. The study sites are indicated by star symbols, and the superimposed numbers indicate the percentage of back-trajectories per cluster for each study site. In order to avoid overloading the figures, the clustered back-trajectories are split by site or by groups of sites: (**a**) Windpoort, Maun Tower, and Reunion; (**b**) Gobabeb and Simonstown; (**c1**–**c3**) Skukuza, Pretoria, and Durban, respectively.

These transports modes were highlighted by Chazette et al. [30] at Henties Bay (180 km from Gobabeb) during the AEROCLO-sA field campaign using the HYSPLIT model. They highlighted three periods with very different transport modes towards Henties Bay. The first mode of transport is associated with Angolan air masses traveling with low AOD (below 0.2) along the Namibian and Angolan coasts. The second transport mode is associated with polluted dust and dust from the Etosha Pan, which is recirculated

above the ocean and has an intermediate AOD value (around 0.4). The third mode is primarily due to direct transport from burning areas in Angola, with an aerosol plume extending vertically between 1.5 and 6 km and a larger AOD (around 0.7). They also observed a possible contribution of forest fire aerosols from South America (south of Brazil, Argentina, and Uruguay) with plumes transported to Henties Bay at around 5–6 km with a contribution to total AOD of 10–15%.

Simonstown and Reunion have similar AOD (0.07 on average), and aerosol type frequencies (MX and CM, and low frequencies of BB/UR aerosols) tend to be affected by long-range transport of biomass burning rather than local biomass burning. Simonstown had a higher frequency of polluted continental/smoke and polluted dust than elevated smoke. Simonstown is impacted by long-range transport from South America, as demonstrated by our findings and consistent with the simulation of aerosol plume across the Atlantic following the 2019 Amazon fires in Bencherif et al. [73]. By contrast, Reunion is located in a pristine area [74] with higher frequencies of elevated smoke and weak anthropogenic influence. As highlighted by Duflot et al. [35], the largest contributions to AOD variability at Reunion are made by biomass burning activity (67.4%) from Southern Hemisphere Africa (21.7%) and Southern Hemisphere South America (19.5%).

According to our results of aerosol classification and back-trajectories, aerosols categorized in the mixed type may arise from various sources, having undergone transformation during their transport. Their optical properties do not allow us to identify them as a precise type. As suggested by Kumar et al. [18], anthropogenic aerosols can be transported from South America and mixed with sea salt, explaining the moderate AOD observed at Skukuza. These aerosols may correspond to the adhesion of fine-mode aerosol to the surface of coarse-mode aerosol, constituting a mixed-type aerosol [37,75]. Due to the predominance of BB/UR aerosols ahead of MX type for sites near biomass burning areas, the MX type is more common for sites far from sources.

4. Conclusions

In this paper, we present an overview and update on the 13 years of observations of aerosol optical properties and types over Southern Africa from ground-based and satellite observations. The key findings are summarized as follows:

- The relationship between AOD and AE allows for the identification of aerosol types, with two types predominating on an annual basis and for the spring season. The BB/UR type is predominantly nearest to biomass burning areas (such as Maun Tower, Windpoort, Skukuza, and Pretoria), with frequencies from 40% to 60%. The MX type is predominant over the remaining sites (accounting for 50–60%).
- Using the vertical distribution of aerosol types from CALIOP, this study highlighted that the vertical profiles of elevated smoke range from 2 to 6 km. Moreover, they behave differently depending on the seasons, with the highest altitude peak during spring (3–4 km) compared with other seasons (2–3 km). Similar to the results obtained with the sun photometer aerosol classification, an increase is found to be associated with sites closer to biomass burning areas.
- Analysis of back-trajectories during the biomass burning season shows that there is intercontinental transport, with air masses coming from South America and the Atlantic Ocean. Moreover, regional transport with air masses coming from South Africa and local recirculation of air masses around the sites was also observed. The height transportation levels vary along each cluster within the altitude range from 1 to 8 km, with the latter representing the highest altitude reached above the Atlantic Ocean.

Observations in this research indicate that the aerosol load observed during the spring is associated with high AOD, AE, and frequency values in BB/UR and elevated smoke. These aerosols seem to originate mainly from biomass burning areas near the study sites and from distant sources, such as Amazonia. The diversity of aerosols in the MX type may reflect a mixture of aerosols from a variety of sources around the sites. It is well known that the mixing processes of an aerosol plume with other types of aerosols (e.g.,

urban pollution and marine aerosols) can significantly impact the optical and chemical composition of the plume [75]. Due to mixing processes, the optical characteristics of the aerosol are modified [37,76]. For some sites, AOD may be enhanced by the mixing of the biomass burning aerosol plume with pollution (Pretoria, Durban, or Skukuza) or mixing with coarse aerosols, such as dust or marine aerosols (Simonstown, Reunion, or Gobabeb).

In general, the results presented in this study support the assumption that BB/UR aerosol variability over the South African region is influenced by its own, as well as Amazonian, biomass burning activities. Torres et al. [77] reported that the peak of biomass burning activity over Southern America is reached generally in August but the season extends through November. Given the temporal coincidence of the biomass burning activity over Southern Africa and Amazonia, we cannot exclude the possibility that Amazonian biomass burning activity could influence the variability of BB/UR aerosols over South Africa [17,30,73]. Discriminating between the contribution of local and distant sources to the variability of biomass burning aerosols requires further investigation and will form the basis of a forthcoming study.

Appendix A

Appendix A.1. Grid Retrieval of CALIOP Observations

Figure A1 represents the 2.0° × 5.0° grid collection of CALIOP observations encompassing the eight sun photometer sites. The red boxes follow the resolution grid of CALIOP L3 data.

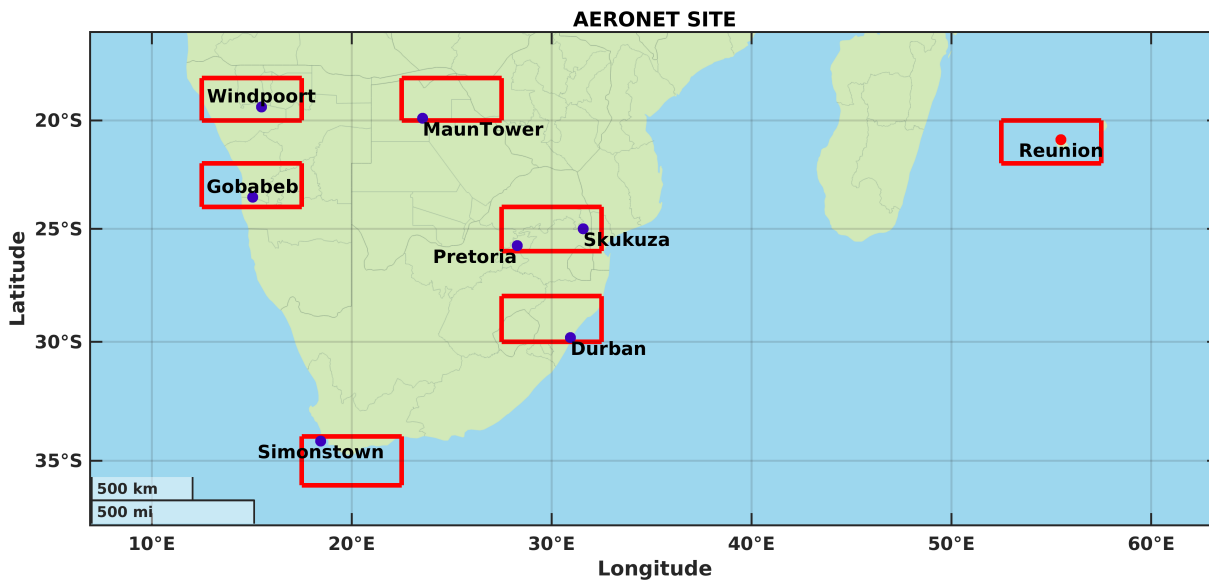**Figure A1.** CALIOP grid retrieval 2.0° × 5.0°, encompassing the eight sun photometer sites.

Appendix A.2. Aerosol Optical Properties: Comparison with Previous Work

Table A1 summarizes the aerosol optical properties at Southern Africa sites as published in the literature and according to our results.

Horowitz et al. [36] and Kumar et al. [18,19] each reported a multiyear annual average AOD value of 0.18 at Skukuza with sun photometer observations over the 1991–2011 and 2005–2006 periods. In the work of Queface et al. [78], the highest AOD value of 0.21 is reported. These three works reported multiyear annual average AE values ranging from 1.34 to 1.47 at 440–870 nm. In our work, we report an AOD average value of 0.19, which is in the middle of those found in previous work. The AE average value of 1.29 is the lowest when compared with previous work. Adesina et al. [24,25] reported multiyear AOD (AE) annual values ranging from 0.11 (1.31) to 0.13 with MODIS-Aqua and -Terra observations at 550 (470–660) nm from 2004 and 2013. For a longer period, our study reports a higher average AOD value (0.15).

Kumar et al. [22,23] reported an AOD (AE) multiyear annual average of 0.23 and 0.24 (150–145) at Pretoria with sun photometer observations at 440 nm (440–870 nm). In our work, we report a lower value of AOD of 0.17 at 550 nm and a higher value of AE of 1.52. As shown by Kumar et al. [23] and in Figure 3b, the AOD decreases when the wavelength decreases. According to this figure, we may consider that our multiyear annual values are consistent with previous work. Kumar et al. [20] and Adesina et al. [24] report AOD multiyear annual values of 0.11 with MODIS observations from 2003–2013 and 2004–2013, respectively. Our work, for another period, shows similar values (0.11).

Kumar et al. [21] reported multiyear AOD annual values of 0.168 to 0.172 at Durban, from MODIS-Terra and -Aqua observations, respectively. These values are higher than those reported by Adesina et al. [24] (0.13) and the value in this work (0.12). This may be due to the difference in datasets. Kumar et al.'s [21] work uses "daily MODIS (Terra and Aqua) Collection 5.1 L2 aerosol products with 10 km × 10 km spatial resolution", while Adesina et al.'s [24] and this work used Level-3 MODIS with a 1° × 1° grid spatial resolution.

Table A1. Comparison of aerosol optical depth (AOD) at Southern Africa sites [18–27,35,36,78,79].

Site	Study Period	Instrument [1]	AOD λ (nm) [2]	AE λ (nm) [2]	Citation
Skukuza	1995–2007	sun photometer	0.21 (500)	1.41 (440–870)	Queface et al. [78]
	1991–2011	sun photometer	0.18 (550)	1.34 (440–870)	Horowitz et al. [36]
	2005–2006	sun photometer	0.18 (500)	1.47 (440–870)	Kumar et al. [18,19]
	1999–2010	sun photometer	0.25 (440)	1.40 (440–870)	Adesina et al. [26]
	2008–2020	sun photometer	0.19 (550)	1.29 (440–870)	present study
	2004–2013	MODIS-T	0.11 (550)	1.31 (470–660)	Adesina et al. [24]
	2004–2013	MODIS-T&A	0.12–0.13 (550)	-	Adesina et al. [25]
	2008–2020	MODIS-T	0.15 (550)	-	present study
Pretoria	2011–2015	sun photometer	0.23 (440)	1.50 (440–870)	Kumar et al. [22]
	2011–2017	sun photometer	0.24 (440)	1.45 (440–870)	Kumar et al. [23]
	2011–2018	sun photometer	0.17 (550)	1.52 (440–870)	present study
	2003–2013	MODIS-T&A	0.11 (550)	0.95 (470–660)	Kumar et al. [20]
	2004–2013	MODIS-T	0.11 (550)	0.94 (470–660)	Adesina et al. [24]
	2011–2018	MODIS-T	0.12 (550)	-	present study
Durban	2003–2013	MODIS-T&A	0.168–0.172(550)	1.38–1.43 (470–660)	Kumar et al. [21]
	2004–2013	MODIS-T	0.13 (550)	1.29 (470–660)	Adesina et al. [24]
	2015–2021	MODIS-T	0.12 (550)	-	present study
	2015–2021	sun photometer	0.17 (550)	1.18 (440–870)	present study
Cape Town	2003–2013	MODIS-T&A	0.08 (550)	1.18 (470–660)	Kumar et al. [20]
	2004–2013	MODIS-T	0.08 (550)	1.18 (470–660)	Adesina et al. [24]
	2015–2021	MODIS-T	0.12 (550)	-	present study
Simonstown	2015–2019	sun photometer	0.075 (500)	0.63 (440–870)	Yakubu et al. [27]
	2015–2021	sun photometer	0.07 (550)	0.70 (440–870)	present study
Gobabeb	2014–2015	sun photometer	0.13 (500)	1.07 (440–870)	Adesina et al. [79]
	2014–2020	sun photometer	0.10 (550)	1.09 (440–870)	present study
	2014–2020	MODIS-T	0.14 (550)	-	present study
Reunion	2007–2012	sun photometer	0.064 (550)	0.70 (440–870)	Horowitz et al. [36]
	2007–2019	sun photometer	0.08 (440)	0.71 (500–870)	Duflot et al. [35]
	2008–2021	sun photometer	0.07 (550)	0.74 (440–870)	present study
	2008–2021	MODIS-T	0.12 (550)	-	present study

[1] MODIS-T: MODIS-Terra platform, MODIS-T&A: MODIS-Terra and Aqua platform; [2] λ (nm): wavelength.

Kumar et al. [20] and Adesina et al. [24] reported the same multiyear annual value of AOD (0.08) at Cape Town from MODIS observations, while our values are higher (0.12). From the sun photometer, the AOD (AE) multiyear average values are (and close to) the same as those reported in Yakubu et al. [27]: 0.07 (0.63–0.70).

Adesisa et al. (2019) reported AOD and AE annual values of 0.13 and 1.07 using sun photometer observations from 2014 to 2015 at Gobabeb. With more years, our work reported a lower AOD value (0.10) and a higher AE value (1.09).

From sun photometer measurements, Duflot et al. [35] reported an AOD multiyear average value of 0.08 at 440 nm and Horowitz et al. [36] reported a lower value of 0.06 at 500 nm. In our work, we report a value of 0.07 at 550 nm, which is in the middle of those found in previous work. AE values reported by each work are in the same order of magnitude, from 0.70 to 0.74.

The slight difference in the multiyear average values of AOD and AE can be due to the different period, the shift in wavelength, and differences in the datasets, particularly for MODIS observations.

Appendix A.3. HYSPLIT Back-Trajectories: Identification of Origin of Air Masses

Figure A2 shows the number of clusters according to the percent of change in total spatial variation (TSV), and Figure A3 presents the height level of each cluster's back-trajectories.

Figure A2. Number of clusters as a function of percent change in total spatial variation (TSV) over the eight sun photometer sites.
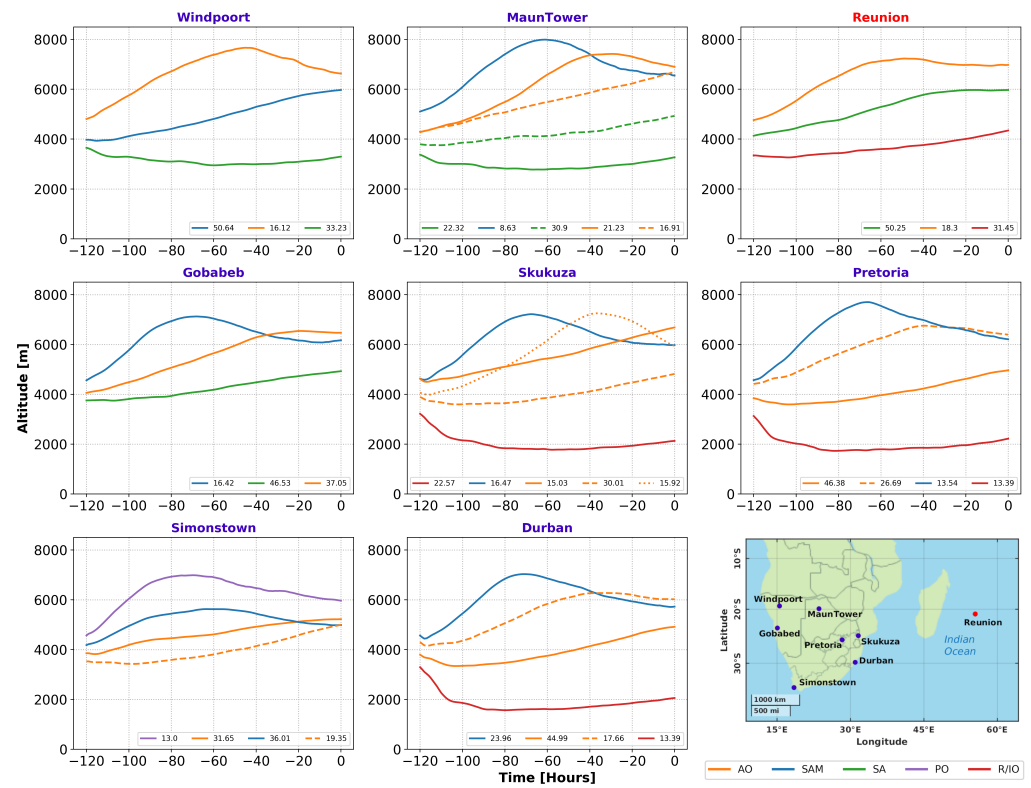

Figure A3. Height level of each back-trajectory cluster over the eight sun photometer sites. Each color is associated with a location: orange for Atlantic Ocean (AO), blue for South America (SAM), green for South Africa (SA), purple for Pacific Ocean (PO), and red for recirculation and Indian Ocean (R/IO).

References

1. de Oliveira Alves, N.; Vessoni, A.T.; Quinet, A.; Fortunato, R.S.; Kajitani, G.S.; Peixoto, M.S.; Hacon, S.D.S.; Artaxo, P.; Saldiva, P.; Menck, C.F.M.; et al. Biomass burning in the Amazon region causes DNA damage and cell death in human lung cells. *Sci. Rep.* **2017**, *7*, 1–13. [CrossRef]
2. Edwards, D.P.; Emmons, L.K.; Gille, J.C.; Chu, A.; Attié, J.L.; Giglio, L.; Wood, S.W.; Haywood, J.; Deeter, M.N.; Massie, S.T.; et al. Satellite-observed pollution from Southern Hemisphere biomass burning. *J. Geophys. Res. Atmos.* **2006**, *111*, D14312 . [CrossRef]
3. Randerson, J.T.; Chen, Y.; van der Werf, G.R.; Rogers, B.M.; Morton, D.C. Global burned area and biomass burning emissions from small fires. *J. Geophys. Res. Biogeosci.* **2012**, *117*, G04012. [CrossRef]
4. van der Werf, G.R.; Randerson, J.T.; Giglio, L.; van Leeuwen, T.T.; Chen, Y.; Rogers, B.M.; Mu, M.; van Marle, M.J.E.; Morton, D.C.; Collatz, G.J.; et al. Global fire emissions estimates during 1997–2016. *Earth Syst. Sci. Data* **2017**, *9*, 697–720. [CrossRef]
5. Giglio, L.; Randerson, J.T.; van der Werf, G.R. Analysis of daily, monthly, and annual burned area using the fourth-generation global fire emissions database (GFED4). *J. Geophys. Res. Biogeosc.* **2013**, *118*, 317–328. [CrossRef]
6. Kganyago, M.; Shikwambana, L. Assessing Spatio-Temporal Variability of Wildfires and their Impact on Sub-Saharan Ecosystems and Air Quality Using Multisource Remotely Sensed Data and Trend Analysis. *Sustainability* **2019**, *11*, 6811. [CrossRef]
7. Garstang, M.; Tyson, P.D.; Swap, R.; Edwards, M.; Kållberg, P.; Lindesay, J.A. Horizontal and vertical transport of air over southern Africa. *J. Geophys. Res. Atmos.* **1996**, *101*, 23721–23736.
8. Lindesay, J.A.; Andreae, M.O.; Goldammer, J.G.; Harris, G.; Annegarn, H.J.; Garstang, M.; Scholes, R.J.; van Wilgen, B.W. International geosphere-biosphere programme/international global atmospheric chemistry SAFARI-92 field experiment: Background and overview. *J. Geophys. Res. Atmos.* **1996**, *101*, 23521–23530.
9. Swap, R.; Privette, J. Overview of the Southern African Regional Science Initiative-SAFARI 2000. In Proceedings of the IEEE 1999 International Geoscience and Remote Sensing Symposium. IGARSS'99 (Cat. No.99CH36293), Hamburg, Germany, 28 June–2 July 1999; Volume 1, pp. 595–597. [CrossRef]
10. Pak, B.C.; Langenfelds, R.L.; Young, S.A.; Francey, R.J.; Meyer, C.P.; Kivlighon, L.M.; Cooper, L.N.; Dunse, B.L.; Allison, C.E.; Steele, L.P.; et al. Measurements of biomass burning influences in the troposphere over southeast Australia during the SAFARI 2000 dry season campaign. *J. Geophys. Res. Atmos.* **2003**, *108*, D138480. [CrossRef]
11. Formenti, P.; D'Anna, B.; Flamant, C.; Mallet, M.; Piketh, S.J.; Schepanski, K.; Waquet, F.; Auriol, F.; Brogniez, G.; Burnet, F.; et al. The Aerosols, Radiation and Clouds in Southern Africa Field Campaign in Namibia: Overview, Illustrative Observations, and Way Forward. *Bull. Am. Meteorol. Soc.* **2019**, *100*, 1277–1298. [CrossRef]
12. Andersen, H.; Cermak, J. First fully diurnal fog and low cloud satellite detection reveals life cycle in the Namib. *Atmos. Meas. Tech.* **2018**, *11*, 5461–5470. [CrossRef]
13. Redemann, J.; Wood, R.; Zuidema, P.; Doherty, S.J.; Luna, B.; LeBlanc, S.E.; Diamond, M.S.; Shinozuka, Y.; Chang, I.Y.; Ueyama, R.; et al. An overview of the ORACLES (ObseRvations of Aerosols above CLouds and their intEractionS) project: Aerosol–cloud–radiation interactions in the southeast Atlantic basin. *Atmos. Chem. Phys.* **2021**, *21*, 1507–1563. [CrossRef]
14. Chang, I.; Gao, L.; Burton, S.P.; Chen, H.; Diamond, M.S.; Ferrare, R.A.; Flynn, C.J.; Kacenelenbogen, M.; LeBlanc, S.E.; Meyer, K.G.; et al. Spatiotemporal Heterogeneity of Aerosol and Cloud Properties Over the Southeast Atlantic: An Observational Analysis. *Geophys. Res. Lett.* **2021**, *48*, e2020GL091469. [CrossRef]
15. Doherty, S.J.; Saide, P.E.; Zuidema, P.; Shinozuka, Y.; Ferrada, G.A.; Gordon, H.; Mallet, M.; Meyer, K.; Painemal, D.; Howell, S.G.; et al. Modeled and observed properties related to the direct aerosol radiative effect of biomass burning aerosol over the southeastern Atlantic. *Atmos. Chem. Phys.* **2022**, *22*, 1–46. [CrossRef]
16. Schmid, B.; Redemann, J.; Russell, P.B.; Hobbs, P.V.; Hlavka, D.L.; McGill, M.J.; Holben, B.N.; Welton, E.J.; Campbell, J.R.; Torres, O.; et al. Coordinated airborne, spaceborne, and ground-based measurements of massive thick aerosol layers during the dry season in southern Africa. *J. Geophys. Res. Atmos.* **2003**, *108*. [CrossRef]
17. Flamant, C.; Gaetani, M.; Chaboureau, J.P.; Chazette, P.; Cuesta, J.; Piketh, S.J.; Formenti, P. Smoke in the river: An Aerosols, Radiation and Clouds in southern Africa (AEROCLO-sA) case study. *Atmos. Chem. Phys.* **2022**, *22*, 5701–5724. [CrossRef]
18. Kumar, K.R.; Sivakumar, V.; Reddy, R.; Gopal, K.R.; Adesina, A.J. Inferring wavelength dependence of AOD and Ångström exponent over a sub-tropical station in South Africa using AERONET data: Influence of meteorology, long-range transport and curvature effect. *Sci. Total. Environ.* **2013**, *461–462*, 397–408. [CrossRef]
19. Kumar, K.R.; Sivakumar, V.; Reddy, R.R.; Gopal, K.R.; Adesina, A.J. Identification and Classification of Different Aerosol Types over a Subtropical Rural Site in Mpumalanga, South Africa: Seasonal Variations as Retrieved from the AERONET Sunphotometer. *Aerosol Air Qual. Res.* **2014**, *14*, 108–123. [CrossRef]
20. Kumar, K.R.; Sivakumar, V.; Yin, Y.; Reddy, R.; Kang, N.; Diao, Y.; Adesina, A.J.; Yu, X. Long-term (2003–2013) climatological trends and variations in aerosol optical parameters retrieved from MODIS over three stations in South Africa. *Atmos. Environ.* **2014**, *95*, 400–408. [CrossRef]
21. Kumar, K.R.; Yin, Y.; Sivakumar, V.; Kang, N.; Yu, X.; Diao, Y.; Adesina, A.J.; Reddy, R. Aerosol climatology and discrimination of aerosol types retrieved from MODIS, MISR and OMI over Durban (29.88°S, 31.02°E), South Africa. *Atmos. Environ.* **2015**, *117*, 9–18. [CrossRef]
22. Kumar, K.R.; Kang, N.; Sivakumar, V.; Griffith, D. Temporal characteristics of columnar aerosol optical properties and radiative forcing (2011–2015) measured at AERONET's Pretoria_CSIR_DPSS site in South Africa. *Atmos. Environ.* **2017**, *165*, 274–289. [CrossRef]

23. Kumar, K.R.; Boiyo, R.; Khan, R.; Kang, N.; Yu, X.; Sivakumar, V.; Griffith, D.; Devi, N.L. Multi-year analysis of aerosol optical properties and implications to radiative forcing over urban Pretoria, South Africa. *Theor. Appl. Climatol.* **2020**, *141*, 343–357. [CrossRef]

24. Adesina, A.J.; Kumar, K.R.; Sivakumar, V. Aerosol-Cloud-Precipitation Interactions over Major Cities in South Africa: Impact on Regional Environment and Climate Change. *Aerosol Air Qual. Res.* **2016**, *16*, 195–211. [CrossRef]

25. Adesina, A.J.; Kumar, K.R.; Sivakumar, V.; Piketh, S.J. Intercomparison and assessment of long-term (2004–2013) multiple satellite aerosol products over two contrasting sites in South Africa. *J. Atmos. Sol.-Terr. Phys.* **2016**, *148*, 82–95. [CrossRef]

26. Adesina, A.J.; Piketh, S.; Kanike, R.K.; Venkataraman, S. Characteristics of columnar aerosol optical and microphysical properties retrieved from the sun photometer and its impact on radiative forcing over Skukuza (South Africa) during 1999–2010. *Environ. Sci. Pollut. Res.* **2017**, *24*, 16160–16171. [CrossRef]

27. Yakubu, A.T.; Chetty, N. Optical properties of atmospheric aerosol over Cape Town, Western Cape of South Africa: Role of biomass burning. *Atmósfera* **2021**, *34*, 395–416. [CrossRef]

28. Kaufman, Y.J.; Haywood, J.M.; Hobbs, P.V.; Hart, W.; Kleidman, R.; Schmid, B. Remote sensing of vertical distributions of smoke aerosol off the coast of Africa. *Geophys. Res. Lett.* **2003**, *30*, 161831. [CrossRef]

29. Swap, R.; Tyson, P. Stable discontinuities as determinants of the vertical distribution of aerosols and trace gases in the atmosphere. *South Afr. J. Sci.* **1999**, *95*, 63–71.

30. Chazette, P.; Flamant, C.; Totems, J.; Gaetani, M.; Smith, G.; Baron, A.; Landsheere, X.; Desboeufs, K.; Doussin, J.F.; Formenti, P. Evidence of the complexity of aerosol transport in the lower troposphere on the Namibian coast during AEROCLO-sA. *Atmos. Chem. Phys.* **2019**, *19*, 14979–15005. [CrossRef]

31. Clain, G.; Baray, J.L.; Delmas, R.; Diab, R.; Leclair de Bellevue, J.; Keckhut, P.; Posny, F.; Metzger, J.M.; Cammas, J.P. Tropospheric ozone climatology at two Southern Hemisphere tropical/subtropical sites, (Reunion Island and Irene, South Africa) from ozonesondes, LIDAR, and in situ aircraft measurements. *Atmos. Chem. Phys.* **2009**, *9*, 1723–1734. [CrossRef]

32. Duflot, V.; Royer, P.; Chazette, P.; Baray, J.L.; Courcoux, Y.; Delmas, R. Marine and biomass burning aerosols in the southern Indian Ocean: Retrieval of aerosol optical properties from shipborne lidar and Sun photometer measurements. *J. Geophys. Res. Atmos.* **2011**, *116*, D18208. [CrossRef]

33. Duflot, V.; Baray, J.L.; Payen, G.; Marquestaut, N.; Posny, F.; Metzger, J.M.; Langerock, B.; Vigouroux, C.; Hadji-Lazaro, J.; Portafaix, T.; et al. Tropospheric ozone profiles by DIAL at Maïdo Observatory (Reunion Island): System description, instrumental performance and result comparison with ozone external data set. *Atmos. Meas. Tech.* **2017**, *10*, 3359–3373. [CrossRef]

34. Verreyken, B.; Amelynck, C.; Brioude, J.; Müller, J.F.; Schoon, N.; Kumps, N.; Colomb, A.; Metzger, J.M.; Lee, C.F.; Koenig, T.K.; et al. Characterisation of African biomass burning plumes and impacts on the atmospheric composition over the south-west Indian Ocean. *Atmos. Chem. Phys.* **2020**, *20*, 14821–14845. [CrossRef]

35. Duflot, V.; Bègue, N.; Pouliquen, M.L.; Goloub, P.; Metzger, J.M. Aerosols on the Tropical Island of La Réunion (21°S, 55°E): Assessment of Climatology, Origin of Variability and Trend. *Remote Sens.* **2022**, *14*, 4945. [CrossRef]

36. Horowitz, H.M.; Garland, R.M.; Thatcher, M.; Landman, W.A.; Dedekind, Z.; van der Merwe, J.; Engelbrecht, F.A. Evaluation of climate model aerosol seasonal and spatial variability over Africa using AERONET. *Atmos. Chem. Phys.* **2017**, *17*, 13999–14023. [CrossRef]

37. Kaskaoutis, D.G.; Badarinath, K.V.S.; Kumar Kharol, S.; Rani Sharma, A.; Kambezidis, H.D. Variations in the aerosol optical properties and types over the tropical urban site of Hyderabad, India. *J. Geophys. Res. Atmos.* **2009**, *114*, D22204. [CrossRef]

38. Patel, P.N.; Dumka, U.; Kaskaoutis, D.; Babu, K.; Mathur, A.K. Optical and radiative properties of aerosols over Desalpar, a remote site in western India: Source identification, modification processes and aerosol type discrimination. *Sci. Total Environ.* **2017**, *575*, 612–627. [CrossRef]

39. Piketh, S.J.; Annegarn, H.J.; Tyson, P.D. Lower tropospheric aerosol loadings over South Africa: The relative contribution of aeolian dust, industrial emissions, and biomass burning. *J. Geophys. Res. Atmos.* **1999**, *104*, 1597–1607.

40. Swap, R.J.; Annegarn, H.J.; Suttles, J.T.; King, M.D.; Platnick, S.; Privette, J.L.; Scholes, R.J. Africa burning: A thematic analysis of the Southern African Regional Science Initiative (SAFARI 2000). *J. Geophys. Res. Atmos.* **2003**, *108*, D138465. [CrossRef]

41. Ginoux, P.; Prospero, J.M.; Gill, T.E.; Hsu, N.C.; Zhao, M. Global-scale attribution of anthropogenic and natural dust sources and their emission rates based on MODIS Deep Blue aerosol products. *Rev. Geophys.* **2012**, *50*, RG3005. [CrossRef]

42. Johansson, L.; Jalkanen, J.P.; Kukkonen, J. Global assessment of shipping emissions in 2015 on a high spatial and temporal resolution. *Atmos. Environ.* **2017**, *167*, 403–415. [CrossRef]

43. Cahoon, D.R., Jr.; Stocks, B.J.; Levine, J.S.; Cofer III, W.R.; O'Neill, K.P. Seasonal distribution of African savanna fires. *Nature* **1992**, *359*, 812–815. [CrossRef]

44. van der Werf, G.R.; Randerson, J.T.; Giglio, L.; Collatz, G.J.; Mu, M.; Kasibhatla, P.S.; Morton, D.C.; DeFries, R.S.; Jin, Y.; van Leeuwen, T.T. Global fire emissions and the contribution of deforestation, savanna, forest, agricultural, and peat fires (1997–2009). *Atmos. Chem. Phys.* **2010**, *10*, 11707–11735. [CrossRef]

45. Adesina, J.A. and Piketh, S.J. *Seasonal Variation of Major Aerosol Types over Skukuza as Inferred from Sunphotometer Measurements*; National Association for Clean Air: Nelspruit, South Africa, 2016; ISBN 978-0-620-70646-9.

46. Eck, T.F.; Holben, B.; Reid, J.; Dubovik, O.; Smirnov, A.; O'neill, N.; Slutsker, I.; Kinne, S. Wavelength dependence of the optical depth of biomass burning, urban, and desert dust aerosols. *J. Geophys. Res. Atmos.* **1999**, *104*, 31333–31349.

47. Dubovik, O.; Sinyuk, A.; Lapyonok, T.; Holben, B.N.; Mishchenko, M.; Yang, P.; Eck, T.F.; Volten, H.; Muñoz, O.; Veihelmann, B.; et al. Application of spheroid models to account for aerosol particle nonsphericity in remote sensing of desert dust. *J. Geophys. Res. Atmos.* **2006**, *111*, D11208. [CrossRef]
48. Ångström, A. The parameters of atmospheric turbidity. *Tellus* **1964**, *16*, 64–75. [CrossRef]
49. Schuster, G.L.; Dubovik, O.; Holben, B.N. Angstrom exponent and bimodal aerosol size distributions. *J. Geophys. Res. Atmos.* **2006**, *111*, D07207. [CrossRef]
50. Hunt, W.H.; Winker, D.M.; Vaughan, M.A.; Powell, K.A.; Lucker, P.L.; Weimer, C. CALIPSO Lidar Description and Performance Assessment. *J. Atmos. Ocean. Technol.* **2009**, *26*, 1214–1228. [CrossRef]
51. Gui, K.; Che, H.; Zheng, Y.; Zhao, H.; Yao, W.; Li, L.; Zhang, L.; Wang, H.; Wang, Y.; Zhang, X. Three-dimensional climatology, trends, and meteorological drivers of global and regional tropospheric type-dependent aerosols: Insights from 13 years (2007–2019) of CALIOP observations. *Atmos. Chem. Phys.* **2021**, *21*, 15309–15336. [CrossRef]
52. Draxler, R.R.; Hess, G. An overview of the HYSPLIT_4 modelling system for trajectories. *Aust. Meteorol. Mag.* **1998**, *47*, 295–308.
53. Hernández-Ceballos, M.; Adame, J.; Bolívar, J.; De la Morena, B. Vertical behaviour and meteorological properties of air masses in the southwest of the Iberian Peninsula (1997–2007). *Meteorol. Atmos. Phys.* **2013**, *119*, 163–175. [CrossRef]
54. Wang, Y.; Zhang, X.; Draxler, R.R. TrajStat: GIS-based software that uses various trajectory statistical analysis methods to identify potential sources from long-term air pollution measurement data. *Environ. Model. Softw.* **2009**, *24*, 938–939. [CrossRef]
55. Millet, T.; Bencherif, H.; Bounhir, A.; Bègue, N.; Lamy, K.; Ranaivombola, M.; Benkhaldoun, Z.; Portafaix, T.; Duflot, V. Aerosol Distributions and Transport over Southern Morocco from Ground-Based and Satellite Observations (2004-2020). *Atmosphere* **2022**, *13*, 923. [CrossRef]
56. Yang, X.; Zhao, C.; Yang, Y.; Fan, H. Long-term multi-source data analysis about the characteristics of aerosol optical properties and types over Australia. *Atmos. Chem. Phys.* **2021**, *21*, 3803–3825. [CrossRef]
57. Bergstrom, R.W.; Pilewskie, P.; Russell, P.B.; Redemann, J.; Bond, T.C.; Quinn, P.K.; Sierau, B. Spectral absorption properties of atmospheric aerosols. *Atmos. Chem. Phys.* **2007**, *7*, 5937–5943. [CrossRef]
58. Russell, P.B.; Bergstrom, R.W.; Shinozuka, Y.; Clarke, A.D.; DeCarlo, P.F.; Jimenez, J.L.; Livingston, J.M.; Redemann, J.; Dubovik, O.; Strawa, A. Absorption Angstrom Exponent in AERONET and related data as an indicator of aerosol composition. *Atmos. Chem. Phys.* **2010**, *10*, 1155–1169. [CrossRef]
59. Giles, D.M.; Holben, B.N.; Eck, T.F.; Sinyuk, A.; Smirnov, A.; Slutsker, I.; Dickerson, R.R.; Thompson, A.M.; Schafer, J.S. An analysis of AERONET aerosol absorption properties and classifications representative of aerosol source regions. *J. Geophys. Res. Atmos.* **2012**, *117*, D17203. [CrossRef]
60. Pace, G.; di Sarra, A.; Meloni, D.; Piacentino, S.; Chamard, P. Aerosol optical properties at Lampedusa (Central Mediterranean). 1. Influence of transport and identification of different aerosol types. *Atmos. Chem. Phys.* **2006**, *6*, 697–713. [CrossRef]
61. Kim, M.H.; Omar, A.H.; Tackett, J.L.; Vaughan, M.A.; Winker, D.M.; Trepte, C.R.; Hu, Y.; Liu, Z.; Poole, L.R.; Pitts, M.C.; et al. The CALIPSO version 4 automated aerosol classification and lidar ratio selection algorithm. *Atmos. Meas. Tech.* **2018**, *11*, 6107–6135. [CrossRef]
62. Alam, K.; Qureshi, S.; Blaschke, T. Monitoring spatio-temporal aerosol patterns over Pakistan based on MODIS, TOMS and MISR satellite data and a HYSPLIT model. *Atmos. Environ.* **2011**, *45*, 4641–4651. [CrossRef]
63. Bègue, N.; Shikwambana, L.; Bencherif, H.; Pallotta, J.; Sivakumar, V.; Wolfram, E.; Mbatha, N.; Orte, F.; Du Preez, D.J.; Ranaivombola, M.; et al. Statistical analysis of the long-range transport of the 2015 Calbuco volcanic plume from ground-based and space-borne observations. *Ann. Geophys.* **2020**, *38*, 395–420. [CrossRef]
64. Vaz Peres, L.; Bencherif, H.; Mbatha, N.; Passaglia Schuch, A.; Toihir, A.M.; Bègue, N.; Portafaix, T.; Anabor, V.; Kirsch Pinheiro, D.; Paes Leme, N.M.; et al. Measurements of the total ozone column using a Brewer spectrophotometer and TOMS and OMI satellite instruments over the Southern Space Observatory in Brazil. *Ann. Geophys.* **2017**, *35*, 25–37. [CrossRef]
65. Jury, M.R.; Buthelezi, M.S. Air Pollution Dispersion over Durban, South Africa. *Atmosphere* **2022**, *13*, 811. [CrossRef]
66. Tripathi, S.N.; Dey, S.; Chandel, A.; Srivastava, S.; Singh, R.P.; Holben, B.N. Comparison of MODIS and AERONET derived aerosol optical depth over the Ganga Basin, India. *Ann. Geophys.* **2005**, *23*, 1093–1101. [CrossRef]
67. Hoelzemann, J.J.; Longo, K.M.; Fonseca, R.M.; do Rosário, N.M.E.; Elbern, H.; Freitas, S.R.; Pires, C. Regional representativity of AERONET observation sites during the biomass burning season in South America determined by correlation studies with MODIS Aerosol Optical Depth. *J. Geophys. Res. Atmos.* **2009**, *114*, D13301. [CrossRef]
68. Hao, W.M.; Ward, D.E.; Susott, R.A.; Babbitt, R.E.; Nordgren, B.L.; Kaufman, Y.J.; Holben, B.N.; Giles, D.M. Comparison of aerosol optical thickness measurements by MODIS, AERONET sun photometers, and Forest Service handheld sun photometers in southern Africa during the SAFARI 2000 campaign. *Int. J. Remote Sens.* **2005**, *26*, 4169–4183.
69. Chu, D.A.; Kaufman, Y.J.; Ichoku, C.; Remer, L.A.; Tanré, D.; Holben, B.N. Validation of MODIS aerosol optical depth retrieval over land. *Geophys. Res. Lett.* **2002**, *29*, MOD2-1–MOD2-4.
70. Bréon, F.M.; Vermeulen, A.; Descloitres, J. An evaluation of satellite aerosol products against sunphotometer measurements. *Remote Sens. Environ.* **2011**, *115*, 3102–3111. [CrossRef]
71. Madry, W.L.; Toon, O.B.; O'Dowd, C.D. Modeled optical thickness of sea-salt aerosol. *J. Geophys. Res. Atmos.* **2011**, *116*, D08211. [CrossRef]

72. Thompson, A.M.; Pickering, K.E.; McNamara, D.P.; Schoeberl, M.R.; Hudson, R.D.; Kim, J.H.; Browell, E.V.; Kirchhoff, V.W.J.H.; Nganga, D. Where did tropospheric ozone over southern Africa and the tropical Atlantic come from in October 1992? Insights from TOMS, GTE TRACE A, and SAFARI 1992. *J. Geophys. Res. Atmos.* **1996**, *101*, 24251–24278.

73. Bencherif, H.; Bègue, N.; Kirsch Pinheiro, D.; Du Preez, D.J.; Cadet, J.M.; da Silva Lopes, F.J.; Shikwambana, L.; Landulfo, E.; Vescovini, T.; Labuschagne, C.; et al. Investigating the Long-Range Transport of Aerosol Plumes Following the Amazon Fires (August 2019): A Multi-Instrumental Approach from Ground-Based and Satellite Observations. *Remote Sens.* **2020**, *12*, 3846. [CrossRef]

74. Mascaut, F.; Pujol, O.; Verreyken, B.; Peroni, R.; Metzger, J.M.; Blarel, L.; Podvin, T.; Goloub, P.; Sellegri, K.; Thornberry, T.; et al. Aerosol characterization in an oceanic context around Reunion Island (AEROMARINE field campaign). *Atmos. Environ.* **2022**, *268*, 118770. [CrossRef]

75. Bègue, N.; Tulet, P.; Pelon, J.; Aouizerats, B.; Berger, A.; Schwarzenboeck, A. Aerosol processing and CCN formation of an intense Saharan dust plume during the EUCAARI 2008 campaign. *Atmos. Chem. Phys.* **2015**, *15*, 3497–3516. [CrossRef]

76. Bègue, N.; Tulet, P.; Chaboureau, J.P.; Roberts, G.; Gomes, L.; Mallet, M. Long-range transport of Saharan dust over northwestern Europe during EUCAARI 2008 campaign: Evolution of dust optical properties by scavenging. *J. Geophys. Res.* **2012**, *117*, D17201. [CrossRef]

77. Torres, O.; Tanskanen, A.; Veihelmann, B.; Ahn, C.; Braak, R.; Bhartia, P.K.; Veefkind, P.; Levelt, P. Aerosols and surface UV products from Ozone Monitoring Instrument observations: An overview. *J. Geophys. Res. Atmos.* **2007**, *112*, D24S47. [CrossRef]

78. Queface, A.J.; Piketh, S.J.; Eck, T.F.; Tsay, S.C.; Mavume, A.F. Climatology of aerosol optical properties in Southern Africa. *Atmos. Environ.* **2011**, *45*, 2910–2921. [CrossRef]

79. Adesina, J.A.; Piketh, S.J.; Formenti, P.; Maggs-Kölling, G.; Holben, B.N.; Sorokin, M.G. Aerosol optical properties and direct radiative effect over Gobabeb, Namibia. *Clean Air J.* **2019**, *29*, 1–11. [CrossRef]